1   **The core Planar Cell Polarity gene, *Vangl2*, maintains apical-basal organisation of the corneal**
2   **epithelium.**

3   D. Alessio Panzica*, Amy S. Findlay*, Rianne van Ladesteijn & J. Martin Collinson†

4   *These authors contributed equally to this work.

5   **† Corresponding author.**

6   J Martin Collinson
7   School of Medical Sciences,
8   University of Aberdeen,
9   Institute of Medical Sciences
10   Aberdeen AB25 2ZD
11   UK
12
13   Email: m.collinson@abdn.ac.uk

14   Running title: Vangl2 in the corneal epithelium

15

16   **ABSTRACT**

17   **The role of the core planar cell polarity (PCP) pathway protein, Vangl2, was investigated in the**

18   **corneal epithelium of the mammalian eye, a paradigm anatomical model of planar cell migration.**

19   **The gene was conditionally knocked out in vivo and knocked down by siRNA, followed by**

20   **immunohistochemical, behavioural and morphological analysis of corneal epithelial cells. The**

21   **primary defects observed in vivo were of apical-basal organisation of the corneal epithelium, with**

22   **abnormal stratification throughout life, mislocalisation of the cell membrane protein, Scribble, to**

23   **the basal side of cells, and partial loss of the epithelial basement membrane. Planar defects in**

24   **migration after wounding and in presence of an applied electric field were noted. However,**

25   **knockdown of Vangl2 also retarded cell migration in individual cells that had no contact with their**

26   **neighbours, which precluded a classic PCP mechanism. It is concluded that some of the planar**

27   **polarity phenotypes in PCP mutants may arise from disruption of apical-basal polarity.**

28

29   Key words: Cornea, epithelium, planar cell polarity, Vangl2, apical-basal polarity

30

31

32   **INTRODUCTION**

33   The cornea is the main refractive constituent of the anterior segment of the vertebrate eye. Its

34   tissue organisation is relatively simple: an outer stratified epithelium representing 10-30% of the

35   corneal thickness (depending on species) sits on a hypocellular collagenous stroma, and an inner

36   endothelial monolayer (Li et al. 1997; Forrester et al. 2002; Henriksson et al. 2009). The structure

37   and transparency of the cornea must be maintained throughout adult life for normal sight.

38   Homeostatic maintenance of the corneal epithelium requires tight control of tissue organisation and

39   cell migration. The corneal and conjunctival epithelia are contiguous and stem cells that maintain

40   the corneal epithelium are located at the boundary between the two – the limbus – around the

41   corneal periphery (Cotsarelis et al. 1996). These limbal epithelial stem cells generate transit

42   amplifying cells that migrate centripetally along the basal layer of the corneal epithelium (Collinson

43   et al. 2002; Nagasaki and Zhao, 2003; Di Girolamo et al. 2015). Proliferative basal corneal epithelial

44   cells may divide several times before losing contact with the basement membrane and

45   differentiating as suprabasal epithelial 'wing cells' (Lehrer & Lavker, 1999). Superficial squamous

46   cells are continuously lost from the corneal epithelial surface e.g. by abrasion. The balance between

47   cell migration into the corneal epithelium, basal cell division and apical cell loss from the corneal

48   surface must be maintained such that the multilayered structure of the corneal epithelium is

49   preserved (Thoft & Friend, 1983; reviewed in Mort et al. 2012).

50   The corneal epithelium exhibits a rigid apical-basal polarity. Cell proliferation is restricted to the

51   basal layer of the corneal epithelium, and apoptosis is normally restricted to desquamating

52   superficial cells (reviewed in Mort et al. 2012). Tight junctions between cells prevent free diffusion

53   across the epithelium and contribute to its protective function (Yi et al. 2000). In addition,

54   desmosomes, gap junctions and immunoglobulin-class cell adhesion molecules connect the cells of

55   the adult corneal epithelium. Hemidesmosomes anchor the basal cells to the underlying basal

56   lamina (Buck, 1982; Smith et al. 2001; Forrester et al. 2002). The corneal epithelium originates as a

57   monolayer during development and in mice stratification occurs neonatally concomitant with eye

58   opening, controlled at least in part by Wnt/β-catenin signalling inhibiting action of bone

59   morphogenetic protein 4 (Zhang et al. 2015).

60   Studies investigating the control of apical-basal polarity have highlighted three complexes whose

61   subcellular localisation directs the internal polarity of epithelial cells in vertebrates or invertebrates:

62   Crumbs and Stardust apically; the Par6/Bazooka/αPKC complex towards the apical side of the lateral

3

63   edge of the cell; and Lethal Giant Larvae, Discs Large and Scribble homologues laterally (Xiao et al.

64   2011; Kumichel & Knust, 2014; Rodriguez-Boulan & Macara, 2014; Whiteman et al. 2014).

65   Planar polarity, i.e. the polarity that epithelial cells exhibit in the plane of their basement membrane,

66   is directed during embryogenesis by a non-canonical branch of the Wnt signalling pathway – the

67   planar cell polarity (PCP) pathway. In invertebrate systems at least this derives from interaction

68   between transmembrane proteins frizzled and van gogh/strabismus, asymmetrically localised to

69   opposite edges of cells, conferring patterns of epithelial cell directionality in the plane of their

70   basement membrane (Taylor et al. 1998; Devenport, 2014). Vertebrates have multiple PCP gene

71   homologues, and PCP pathways have multiple functions during embryogenesis (Lu et al. 2004; Gao

72   et al. 2011; Mao et al. 2011; Wansleeben & Meijlink, 2011; Wallingford, 2012). Although

73   extrapolation between vertebrate and invertebrate systems is not straightforward, mutation of the

74   *van gogh* homologue, *Vangl2*, in vertebrate embryos ablates all PCP signalling and produces heart,

75   inner ear and neural tube defects consistent with failure of cell directionality and migration (Greene

76   et al. 1998; Henderson et al. 2001; Kibar et al. 2001; Murdoch et al. 2001; Park & Moon, 2001; Goto

77   & Keller, 2002; Monticouquiol et al. 2003; Phillips et al. 2005; Roszko et al. 2009; Lei et al. 2010;

78   Yates et al. 2010; Ramsbottom et al. 2014).

79   There is evidence of interaction between apical-basal and planar polarity pathway components.

80   Apical localisation of PCP proteins is critical for their function (Das et al., 2014), and protein kinase C

81   alpha (αPKC), part of the Par6/Bazooka/αPKC complex which characterises the apical-lateral side of

82   the cell, can inhibit Frizzled-PCP signalling in Drosophila by phosphorylating Frizzled and thereby

83   stopping it from signalling (Djiane et al. 2005). Par3 (Bazooka) and Scribble have been linked to

84   defects in asymmetric cell division and cell polarity defects (Lin et al. 2000). Scribble protein is key to

85   potential interactions between apical/basal and planar polarity. Within Drosophila, scribble binds

86   van gogh protein (also known as strabismus) via its PDZ domain 3 and cooperates in establishing PCP

87   (Coubard et al. 2009). In addition heterozygous *scribble* mutations were found to exacerbate PCP

88   defects of *van gogh* (*vang*) mutants, whereas Discs Large and Lethal Giant Larvae, the other proteins

89   located with Scribble along the baso-lateral edge of cells, did not, indicating a specific role for

90   Scribble in Drosophila PCP (Courbard et al. 2009). The *scribble*[5] mutation, encoding a protein

91   truncated before the 3rd PDZ domain, exhibited PCP defects in wing cell alignment, but not apical-

92   basal polarity defects (Courbard et al. 2009).

93   In vertebrates the 3rd and 4th PDZ domains of Scribble bind the C-terminus of Vangl2 and this

94   interaction is required for asymmetric localisation of Vangl2 in cochlear hair cells (Monticouquiol et

95   al. 2006). *Vangl2*$^{Lp/+}$ *Scribble*$^{Crc/+}$ double mutants show cochlea PCP defects akin to those observed in

96   *Vangl2*$^{Lp/Lp}$ mutants indicating that Scribble and Vangl2 proteins work in the same genetic pathway

97   during PCP cell alignment (Monticouquiol et al. 2003). Hence Scribble, although having a canonical

98   role in establishment of apical/basal polarity, also has a role in the establishment of PCP in

99   vertebrates, regulating cell cohesion junctional complex maintenance (Yates et al. 2013).

100   Little work has been done on PCP gene function in adult vertebrate tissues. As part of a study

101   investigating the control of patterning in the corneal epithelium, we conditionally knocked out the

102   core PCP gene *Vangl2* in the corneal epithelium, and were able to show classic planar polarity

103   defects – Vangl2 acted through PCP intermediates Dishevelled, DAAM1 and ROCK1/2, modulating

104   corneal epithelial cell cytoskeletal rearrangement, cell alignment and migration (in vivo and in vitro)

105   (Findlay et al. 2016). Here we describe also a severe disruption of apical-basal polarity with failure of

106   basal cells to maintain a normal basement membrane. The data show PCP genes interact with apical-

107   basal pathways in adult vertebrate system and that Vangl2 activity is required for normal

108   stratification of the corneal epithelium.

109

110 **Materials and Methods**

111 **Mice**

112 Hemizygous *Tg(Pax6-cre, GFP)1Pgr* transgenic mice (henceforth '*Le-Cre*$^{Tg/-}$') drive *Cre* recombinase

113 expression in the lens and corneal epithelia (Williams et al. 1998; Ashery-Padan et al. 2000). *Le-*

114 *Cre*$^{Tg/-}$, *Vangl2*$^{Lp/+}$ and *Vangl2*$^{fl/fl}$ floxed mice (Ramsbottom et al. 2013) were maintained on a

115 congenic CBA/Ca genetic background. All animal procedures were carried out according to Animals

116 (Scientific Procedures) Act 1986 and were passed by University of Aberdeen Ethical Review Board.

117

118 Due to lethality of the *Vangl2*$^{Lp/Lp}$ homozygous mutants (Strong & Hollander, 1949), Cre-*lox*P

119 technology (Gu et al. 1994) was used to delete *Vangl2* conditionally in the corneal epithelium of *Le-*

120 *Cre*$^{Tg/-}$*; Vangl2*$^{fl/fl}$ animals. *Vangl2*$^{fl/fl}$ animals were mated with *Le-Cre*$^{Tg/-}$ mice and their genotypes

121 were confirmed by polymerase chain reaction (PCR) using primers and conditions described in

122 Findlay et al. (2016). The Le-Cre transgene is active from E8.75 in the lens placode and is expressed

123 continuously throughout the lens and corneal epithelium (Ashery-Padan et al. 2000). *Le-Cre*$^{Tg/-}$*;*

124 *Vangl2*$^{fl/+}$ from F1 were backcrossed with *Vangl2*$^{fl/fl}$ mice to obtain *Le-Cre*$^{Tg/-}$*; Vangl2*$^{fl/fl}$ mice and *Le-*

125 *Cre*$^{Tg/-}$*; Vangl2*$^{fl/+}$ littermate controls. *Le-Cre*$^{-/-}$ *Vangl2*$^{fl/fl}$ animals were normal and exhibited no

126 looptail defects, indicating the floxed allele was neutral and the Le-Cre transgene was not showing

127 leaky expression in the germline. Mice were killed by cervical dislocation, their eyes enucleated and

128 fixed for processing.

129

130 **Cell Culture**

131 *In vitro* experiments were carried out by using an immortalised human corneal epithelium cell line

132 (HCE-S) donated by Julie Daniels, Institute of Ophthalmology (Notara & Daniels, 2010). Cells were

133 maintained in DMEM/F-12 media (Life Technologies), 10% fetal calf serum (FCS) (Invitrogen), 1%

134 Penicillin Streptomycin solution (10,000 units penicillin and 10 mg streptomycin/ml)(Sigma) at 37°C

135 in a humidified atmosphere of 5% CO_2. Culture medium was replenished every 72 hours.

136 A robust knockdown of VANGL2 to ~30% of normal levels was obtained in transfected HCE cells

137 using 10 nM HPP grade Vangl2_5 siRNA 5'-UAGAAUUAGGAAGUACCCAUA-3' as described in Findlay

138 et al. (2016). In brief, 60,000 cells were seeded in each well of a 24-well plate in 0.1 ml of culture

139 media. Cells were incubated under their normal growth condition while 75 ng siRNA was diluted

140 down in 100 μl of serum-free culture medium to a final concentration of 10 nM. The diluted siRNA

141   was mixed with 3 μl of HiPerFect transfection reagent and incubated for 10 minutes at room

142   temperature before adding drop-wise to HCE cells. After 3 hours incubation of with the transfection

143   complexes 400 μl of culture medium were added in each well. Cells were passage 24 h later for

144   experiments.

145   **Cellular migration studies upon application of electric fields**

146   Following gene silencing with siRNAs HCE cells were exposed to physiological electric field

147   stimulation to measure forward migration index and directionality of electrotactic movement.

148   Control and knockdown HCE cells were harvested from 24-well plate by addition of trypsin-EDTA,

149   spun and re-suspended in 500 μl of culture media. Cells were seeded into 'ibidi' 15 μm

150   chamber-slides (Thistle Scientific) and time-lapse video recording performed, using a Nikon Diaphot

151   inverted phase contrast microscope with a temperature-controlled environment chamber in a direct

152   current 200 mV/mm electric field by adopting a set-up previously described by Rajnicek et al. (2006).

153

154   A measure of planar-oriented migration, the forward migration index (FMIX) was measured by using

155   the   'Manual   Tracking'   and   'Chemotaxis'   plugins   (available   at

156   http://rsbweb.nih.gov/ij/plugins/index.html) for ImageJ. FMIX is one of the most indicative

157   measures of migration and is determined by measuring, for each cell, the movement along the x axis

158   (x) as a proportion of the total migration distance (d), evaluating the magnitude of the directional

159   cell movement towards the cathode. Conventionally, the cathode is to the left, so the closer the

160   value of FMIX to -1 the more directed is migration to the cathode on average.   FMIX was measured

161   separately for individual cells in culture and cells as part of confluent sheets.

162

163   **Histology**

164   Eyes were enucleated from adult animals killed by a Schedule 1 procedure and fixed in

165   paraformaldehyde (4% in phosphate buffered solution, PBS) for 4-6 hours at 4°C prior processing for

166   paraffin embedding.

167   Eyes were washed 3 times in PBS, 20 minutes, then for 15 minutes in saline solution (0.9% NaCl).

168   Eyes were then dehydrated through a series of 15 minutes ethanol changes (70%, 85%, 95% and

169   100%) before being cleared with xylene (2 x 5 minutes washes at room temperature and incubation

170   overnight in fresh xylene) and embedding in paraffin wax. 7 μm-thick sections were cut in the

171   transverse plane.

Haematoxylin and eosin staining

173 Wax sections were deparaffinised in Histoclear (HS-200, National Diagnostics), 2 x 10 minutes and

174 washed 2 x 5 minutes in 100% ethanol. Rehydration in a serial change of ethanol washes for 5

175 minutes each (95%, 85% and 70% ethanol) followed. Slides were then washed with PBS, incubated in

176 Gill's haematoxylin solution for 1 minute and washed in tap water. Slides were washed in Scott's tap

177 water (20g/L $MgSO_4.7H_2O$, 20g/L $NaHCO_3$), rinsed with tap water and incubated for 30 seconds in

178 eosin solution (1% eosin in 50% ethanol-5mM acetic acid). Slides were then dehydrated an ethanol

179 series, cleared in xylene and mounted with Di-n-butylphthalate in xylene (DPX). Imaging was

180 performed using a Nikon E400 Eclipse light microscope in bright field.

181

Immunohistochemistry

183 Detection of PCP proteins in the corneal tissue and HCE cells was carried out by

184 immunohistochemistry using material and reagents as described in Findlay et al. (2016). Primary

185 antibodies were: BrdU, ab181664 (Abcam); Scribble sc-28737 (Santa Cruz), PI3K, #4252 (Cell

186 Signalling Technology); laminin, ab11575 (abcam); PAX6 (Developmental Studies Hybridoma Bank),

187 mouse monoclonal '4A4' recognizing ΔN-P63 (Santa Cruz); cytokeratin-12 (Santa Cruz). Secondary

188 antibodies were: (all Molecular Probes) Alexa 488-conjugated goat anti-mouse IgG1 A21121; Alexa

189 568-conjugated donkey anti-mouse IgG A10037; Alexa 488-conjugated rabbit anti-goat IgG A110178;

190 Alexa 594-conjugated donkey anti-rabbit IgG A21207. Confocal LSM700-Zeiss Imager M2 Upright

191 and Nikon 400 Eclipse Microscopes were used to image fluorescent sections.

192

Immunofluorescence on whole-mount corneas

194 Corneas were dissected from fixed eyeballs of adult animals. Dissected corneas were washed in PBS,

195 3 x 10 minutes, permeabilised in methanol for 20 minutes at -20°C and washed 3 x 10 minutes with

196 PBS. Corneas were incubated with 1% pepsin in 10 mM HCl for 15 minutes at 37°C, neutralised in 0.1

197 M sodium borate buffer, pH 8, for 10 minutes and washed 2 x 10 minutes with PBS. Antigen retrieval

198 was achieved by treating the corneas with 1% sodium dodecyl sulphate in PBS for 5 minutes and

199 washed 3 x 5 minutes with PBS. Primary and secondary antibodies incubations followed as described

200 previously and then corneas were flattened by 4 scalpel incisions and mounted in fluorescence

201   mounting medium with the corneal epithelium facing upwards. Confocal LSM700-Zeiss Imager M2

202   Upright and Nikon 400 Eclipse Microscopes were used for imaging.

203

204   **Apoptosis assay**

205   The Terminal deoxynucleotidyl transferase dUTP nick end labelling (TUNEL) In Situ Cell Death

206   Detection kit-(fluorescein) (Roche, UK) was used to label apoptotic cells in the corneal epithelium of

207   tissue sections. Deparaffinised sections were incubated with proteinase K (80 µg/mL) for 5 minutes

208   at room temperature and then washed in PBS. A positive control slide was treated with DNAase1 [50

209   units/mL DNAase 1 in 50 mM Tris-HCl pH 7.5, 1mM $MgCl_2$, 1 mg/mL bovine serum albumen (BSA)]

210   for 30 minutes at 37 $^{\circ}$C. TUNEL labelling was performed by incubating slides with coverslips with the

211   TUNEL reaction mixture according to manufacturer's instructions for 60 minutes at 37°C in the dark.

212   A negative control was included in each experimental set up by incubating fixed and permeabilized

213   tissue in 50 µL Label solution without enzyme. Slides were then washed 3 x 5 minutes in PBS,

214   mounted in Vectashield and viewed under a Nikon Eclipse E400 fluorescence microscope.

215

216   **Morphometric measurements of the cornea**

217   Images of sagittal adult eye sections of $Le\text{-}Cre^{Tg/\text{-}}$; $Vangl2^{fl/fl}$ and $Le\text{-}Cre^{Tg/\text{-}}$; $Vangl2^{fl/+}$ animals

218   following H&E staining were captured by a digital camera (Qimaging, QICAM Fast1394) at 400x

219   magnification and morphometric measurements of the corneal epithelium thickness were made

220   with ImageJ (available online at http://imagej.nih.gov/ij/). The method of Ramaesh et al. (2003) was

221   used to measure the thickness of the corneal epithelium and the whole cornea. In brief,

222   measurements were made in three different areas (two peripheral and one central) in the five

223   central serial sections of each adult eye.   Mean thicknesses were calculated for the peripheral

224   regions of each section and used to calculate mean thickness in each eye.

225

226   Corneal diameters were measured using a stereomicroscope. An image of the eye was taken

227   alongside a calibrated ruler and measurements of the corneal diameter were made.

228

229   **Transmission Electron Microscopy**

230   For transmission electron microscopy, eyes were collected and fixed in 2% gluteraldehyde for 4

231   hours. The corneas were dissected and the tissue post-fixed in osmium, dehydrated through

232   increasing concentrations of ethanol and propylene oxide, embedded in plastic and semi-thin

233   sections cut tetroxide at the Histology Facility (Institute of Medical Sciences, University of

234   Aberdeen). The sections were mounted on copper grids, stained with lead citrate and uranyl acetate

235   before imaging on a JEOL 1400 plus transmission electron microscope.

236

237   **Cell proliferation study**

238   *Le-Cre*$^{Tg/-}$*; Vangl2*$^{fl/fl}$ and *Le-Cre*$^{Tg/-}$; *Vangl2*$^{fl/+}$ adult littermates were given a single intraperitoneal

239   injection of 10 mg/mL bromodeoxyuridine (BrdU) in sterile PBS, and killed 2 hours later be cervical

240   dislocation. Eyes were enucleated and processed for immunohistochemistry as above.

241

242   **Statistical analysis**

243   For normally distributed data, a 2-tailed unpaired *t*-test was used in most cases to determine

244   statistical significance when comparing results obtained from *Le-Cre*$^{Tg/-}$; *Vangl2*$^{fl/fl}$ and *Le-Cre*$^{Tg/-}$;

245   *Vangl2*$^{fl/+}$ littermates or V2_*KD* and NT control cells. Mann-Whitney U was used for nonparametric

246   data to compare between genotypes. One way analysis of variance (ANOVA) was used when three

247   or more groups of data were compared, with post-hoc Tukey HSD test to identify significant

248   difference between pairs of groups.

249

250

251

252

253

254

255 **RESULTS**

256

257 **Ablation of *Vangl2* results in abnormal stratification of the corneal epithelium**

258 Multiple PCP genes including *Vangl2* have been shown by RT-PCR, immunohistochemistry and

259 western blot to be expressed in the murine corneal epithelium (Findlay et al. 2016). The eyes of

260 adult 'loop tail' mice that are heterozygous for an inactivating mutation in *Vangl2* (*Vangl2$^{Lp/+}$*) were

261 grossly normal, but tissue sectioning revealed mild corneal defects, with disruption of epithelial

262 stratification and irregularities of basal cell nuclei seen in all corneas that were not observed in their

263 wild-type littermates (Figure 1A, B) (n = 8). *Vangl2^{Lp}* is a semi-dominant allele and *Vangl2$^{Lp/Lp}$* mice

264 die during embryogenesis or shortly after birth with severe neural tube defects (Strong and

265 Hollander, 1949; Yin et al., 2012; Chen et al., 2013). In order to study the role of Vangl2 in the adult

266 corneal epithelium, a conditional knockout was made by breeding *Vangl2*-floxed mice (*Vangl2$^{fl/fl}$*) to

267 *Le-Cre$^{Tg/-}$* mice expressing Cre in the lens and corneal epithelia (Ashery-Padan et al. 2000;

268 Ramsbottom et al. 2014). The progeny of these matings were backcrossed onto the *Vangl2$^{fl/fl}$* line to

269 generate *Le-Cre$^{Tg/-}$ Vangl2$^{fl/+}$* and *Le-Cre$^{Tg/-}$ Vangl2$^{fl/fl}$* littermates (as well as *Le-Cre$^{-/-}$ Vangl2$^{fl/+}$* and *Le-*

270 *Cre$^{-/-}$ Vangl2$^{fl/fl}$* control mice). Haematoxylin and eosin staining of adult *Le-Cre$^{Tg/-}$ Vangl2$^{fl/fl}$* eyes

271 revealed a highly disrupted stratification of the corneal epithelium that was not observed in *Le-*

272 *Cre$^{Tg/-}$ Vangl2$^{fl/+}$* controls (n > 24) (Figure 1C-E). Sections revealed patches of both abnormally thin

273 (Figure 1D) and abnormally thick corneal epithelium (Figure 1E). Thin regions of the epithelium were

274 composed of as little as one or two cellular layers with no consistent cellular morphology, and were

275 sharply juxtaposed with epithelium of normal thickness (5-7 cells) or hypertrophic epithelium up to

276 10 cells thick. In *Le-Cre$^{Tg/-}$ Vangl2$^{fl/+}$* controls (n = 24) and all *Le-Cre$^{-/-}$* corneas (n = 40) the epithelium

277 was uniform and smooth, 5-7 cells thick.

278 Stratification of the corneal epithelium is a postnatal event (Zieske et al. 2004). While the corneal

279 epithelia of both *Vangl2*-null and control mice were monolayers during embryogenesis, and the

280 epithelia were morphologically normal to birth examination of corneas from neonatal mice showed

281 that stratification of the epithelium was delayed in the mutants. At postnatal day 5, in contrast to

282 *Le-Cre$^{-/-}$ Vangl2$^{fl/+}$* , *Le-Cre$^{-/-}$ Vangl2$^{fl/fl}$* and *Le-Cre$^{Tg/-}$ Vangl2$^{fl/+}$* control mice whose epithelium was

283 typically 2-3 cells thick, the epithelium of *Le-Cre$^{Tg/-}$ Vangl2$^{fl/fl}$* mice was a monolayer, and in some

284 areas only a thin cytoplasmic covering was visible (n = 9) (Figure 2).

285   ***Vangl2*-null corneas exhibit reduced or partially absent corneal epithelium basement membrane**

286   Histological analysis (Figure 1) suggested the normal basal/wing/squamous cell apical-basal

287   arrangement of the epithelium was disrupted in *Le-Cre*$^{Tg/-}$ *Vangl2*$^{fl/fl}$ corneas, compared to controls.

288   The basement membrane of mutant corneal epithelia was disrupted and sometimes undetectable in

289   mutant corneal epithelia – this was apparent by haematoxylin and eosin staining (n > 25), and

290   immunohistochemistry using antibodies against extracellular matrix proteins laminin and collagen

291   IV. Partial or total absence of collagen IV and laminin was reproducibly observed in *Le-Cre*$^{Tg/-}$

292   *Vangl2*$^{fl/fl}$ corneal epithelial (n = 6) but not in the controls (n = 9) (Figure 3; Supplementary Figure 1).

293   A preliminary transmission electron microscope (TEM) analysis of *Le-Cre*$^{Tg/-}$ *Vangl2*$^{fl/fl}$ corneas (n = 2)

294   was performed alongside control littermates, *Le-Cre*$^{Tg/-}$ *Vangl2*$^{fl/+}$ (n = 2) and *Le-Cre*$^{-/-}$ *Vangl2*$^{fl/fl}$ (n = 2)

295   which confirmed disruption of the basement membrane. Control *Le-Cre*$^{Tg/-}$ *Vangl2*$^{fl/+}$ and *Le-Cre*$^{-/-}$

296   *Vangl2*$^{fl/fl}$ eyes both exhibited a distinct basement membrane underlying the corneal epithelium and

297   also a clear morphological difference in cell shape and cytoplasm density between the polarised

298   basal epithelial cells and the overlying apical cells (Supplementary Figure 2). Strikingly the basement

299   membrane was also much thinner in the *Le-Cre*$^{Tg/-}$ *Vangl2*$^{fl/fl}$ mutant corneas and partially absent.

300   Cells in the mutant corneas were arranged in a disorganised manner, there was no clear

301   morphological differentiation between basal and apical cells, and the basal cells showed the same

302   cytoplasmic density as more superficial cells (Supplementary Figure 2).

303

304   **Morphometric analysis of mutant corneas**

305   A morphometric analysis was performed on *Le-Cre*$^{Tg/-}$ *Vangl2*$^{fl/fl}$ corneas and controls. Mean

306   diameter of *Le-Cre*$^{Tg/-}$ *Vangl2*$^{fl/fl}$, *Le-Cre*$^{Tg/-}$ *Vangl2*$^{fl/+}$ and *Cre*$^{-/-}$ corneas was measured. Consistent with

307   previous studies showing that Cre expression is not always neutral to phenotype, it was found that

308   *Le-Cre*$^{Tg/-}$ eyes are smaller than Cre-negative eyes, irrespective of *Vangl2*-genotype (Adams and van

309   der Weyden, 2001; Dorà et al. 2014) (Figure 4A). This is presumed to be either a toxic effect of Cre

310   or, more likely, a negative effect of reduced Pax6 availability due to Pax6 binding sites in the *Le-Cre*

311   promoter. For this reason, only *Le-Cre*$^{Tg/-}$ *Vangl2*$^{fl/+}$ mice were used as controls for morphometric

312   analysis.

313   Transverse medial sections from serially sectioned eyes were stained with haematoxylin and eosin

314   and the thickness of the corneal epithelium was measured in central and peripheral regions as

315   described in the Methods sections. On average the epithelium of *Le-Cre*$^{Tg/-}$; *Vangl2*$^{fl/fl}$ corneas was

316   significantly thicker in both central and peripheral regions when compared with *Le-Cre*$^{Tg/-}$; *Vangl2*$^{fl/+}$

317   controls (central corneal epithelium thickness ± SEM: *Le-Cre*^{*Tg/-*}*; Vangl2*^{*fl/+*} 25.85 ± 2.15 μm, *Le-Cre*^{*Tg/-*}*;*

318   *Vangl2*^{*fl/fl*} 41.61 ± 6.76 μm. *t*-test: n = 10; *P* = 0.0396. Peripheral corneal epithelium thickness ± SEM:

319   *Le-Cre*^{*Tg/-*}*; Vangl2*^{*fl/+*} 25.55 ± 1.43 μm, *Le-Cre*^{*Tg/-*}*; Vangl2*^{*fl/fl*} 37.62 ± 4.72 μm. *t*-test: n = 10; *P* = 0.0157)

320   (Figure 4B).

321   On the basis of these data it was suggested that one of the primary defects in corneal epithelia that

322   are null for *Vangl2*, and which should therefore lack all PCP signalling, may in fact be a failure of

323   normal apical-basal epithelial polarity. Further molecular analysis was performed on mutant corneas

324   and controls to investigate this.

325

326

327   **Cell proliferation and cell death in the corneal epithelia of *Vangl2*-deficient mice**

328   In normal corneal epithelia, cell proliferation is restricted to the basal cell layer, and apoptotic

329   events are normally only detected in superficial apical cells prior to desquamation. It was

330   considered possible that the defects observed above may result from loss of apical and basal identity

331   of cells in which case patterns of proliferation and apoptosis may be disrupted. TUNEL labelling was

332   therefore performed to label apoptotic cells in the corneal epithelium of *Le-Cre*^{*Tg/-*}*; Vangl2*^{*fl/fl*} mice

333   and *Le-Cre*^{*Tg/-*}*; Vangl2*^{*fl/+*} control animals. Apoptotic nuclei were restricted to cells in the superficial

334   layer of both control and *Le-Cre*^{*Tg/-*}*; Vangl2*^{*fl/fl*} corneas. No TUNEL-positive cells were detected in the

335   basal or wing layers of the corneal epithelium in either *Vangl2*-deficient or control mice (Figure 5),

336   which reflects normal shedding from the epithelial surface (Ren and Wilson 1996).

337   To examine whether disrupted stratification of the corneal epithelium in *Vangl2*-deficient corneal

338   epithelia was linked to defects in epithelial cell proliferation, bromodeoxyuridine (BrdU) staining was

339   performed in order to observe proliferating cells within the corneal epithelium. Mice were treated

340   with a single intraperitoneal injection of BrdU, to label cells in S-phase, for 2 hours before the mice

341   were killed and eyes taken for BrdU immunohistochemistry. In both *Le-Cre*^{*Tg/-*} *Vangl2*^{*fl/fl*} mice eyes,

342   *Le-Cre*^{*Tg/-*} *Vangl2*^{*fl/+*} and all *Le-Cre*^{*-/-*} controls (n = 6-12 of each genotype), BrdU incorporation was

343   restricted to cells in the basal layer of the epithelium only (Figure 5 D, E). No suprabasal DNA

344   synthesis was observed within mutant mice and therefore no evidence of loss in apical-basal

345   controlled mitotic division.

346   These data suggest that although the morphological differentiation between apical and basal

347   epithelial cells was often lost in *Le-Cre*^{*Tg/-*} *Vangl2*^{*fl/fl*} corneas, cell identity (basal or apical) was

348   maintained and hence proliferation continued to be restricted to the basal layer and apoptosis to

349   the superficial cell layers.

350

351   **Localisation of apical-basal and cell fate markers in the control and mutant corneal epithelium**

352   The basal lamina is secreted by corneal epithelial cells, so the disruption of the basement membrane

353   in *Vangl2*-null corneas could result from defective subcellular apical-basal organisation. The

354   membrane-associated scaffold protein Scribble has been previously described as an important

355   apical-basal organiser within Drosophila cells through its role, along with the other proteins in its

356   complex, Discs large and Lethal Giant Larvae, in the subcellular localisation of proteins (Bilder and

357   Perrimon*,* 2000; Harris & Lim, 2001). *Scribble* has previously been shown to be expressed within the

358   corneal epithelium of mice (Nguyen et al. 2005). In order to further study apical-basal polarity in the

359   conditional *Vangl2*-knockout corneas, Scribble immunostaining was performed on *Le-Cre*$^{Tg/-}$

360   *Vangl2*$^{fl/fl}$ eyes and compared to *Le-Cre*$^{Tg/-}$ *Vangl2*$^{fl/+}$ littermates. Scribble was found to be localised

361   primarily to the lateral and apical boundaries of the basal epithelial cells of control *Le-Cre*$^{Tg/-}$

362   *Vangl2*$^{fl/+}$ mice, and was generally absent from the basal plasmamembrane of these cells (Figure 6)

363   (n = 5 corneas). In *Le-Cre*$^{Tg/-}$ *Vangl2*$^{fl/fl}$ eyes Scribble localisation was moderately but consistently

364   disrupted, with localisation bleeding into the basal boundary of many cells (n = 5 corneas) (Figure

365   6B). This suggests disruption of apical-basal polarity in those cells, associated with partial or total

366   loss of the basement membrane described above. Phosphatidylinositol-4,5-bisphosphate 3-kinase

367   (PI3K) is an important enzyme for corneal epithelial cellular motility and intracellular trafficking

368   (Zhao et al. 2006). It is activated by growth factors acting upon cells and initiating signalling through

369   downstream effectors such as protein kinase B (Katso et al. 2001). Xu et al. (2010) grew mammary

370   epithelial cells upon a laminin-rich ECM; cells grown on the ECM became polarised and displayed a

371   localisation of PI3K to the basal side. Cells grown in the absence of laminin remained unpolarised

372   with no localisation of PI3K in the cell. Immunohistochemistry was performed to investigate PI3K

373   localisation in control and mutant corneal epithelia and to determine whether loss of the basement

374   membrane affected distribution of the protein. When *Le-Cre*$^{Tg/-}$ *Vangl2*$^{fl/fl}$ mice (n = 3) were

375   compared to *Le-Cre*$^{Tg/-}$ *Vangl2*$^{fl/+}$ littermates (n = 5), fluorescence was highest in the cytoplasm or cell

376   membranes of basal cells of *Le-Cre*$^{Tg/-}$ *Vangl2*$^{fl/+}$ mice eyes as expected, however *Le-Cre*$^{Tg/-}$ *Vangl2*$^{fl/fl}$

377   eyes exhibited only low protein levels in basal cells, similar to that observed in more apical cells

378   (Figure 6).

379   Further markers of cell fate and apical-basal identity were assayed in mutant corneas.

380   Immunohistochemical analysis of localisation of the ΔN isoform of the tumour suppressor protein

381   P63, previously shown to be a marker of basal corneal epithelial cells in the mouse (Collinson et al.,

382   2002; Ramaesh et al., 2005), revealed no difference between control *Le-Cre*$^{Tg/-}$ *Vangl2*$^{fl/+}$ (n = 4) and

383   mutant *Le-Cre*$^{Tg/-}$ *Vangl2*$^{fl/fl}$ eyes (n = 3), with basal cells of both genotype exhibiting strong staining

384   and apical cells very weak or no staining. The definitive corneal epithelial marker, cytokeratin-12,

385   was localised to cytoplasm of all cells in all corneal epithelia, irrespective of genotype (n = 4 of each),

386   and the ocular surface marker, Pax6, was localised to nuclei of all cells (n = 4 of each genotype)

387   (Figure 6). Loss of either of these markers would suggest failure of corneal epithelial identity.

388   These data, together with the defects to the basement membrane described above, suggested that

389   there was no loss of corneal epithelial identity in the *Le-Cre*$^{Tg/-}$ *Vangl2*$^{fl/fl}$ mutants, but that the basal

390   epithelial cells had partially or totally lost their apical-basal polarity.

391

392   **Loss of *Vangl2* causes cells to exhibit migration defects**

393   Wound healing efficiency in embryonic skin is regulated by a PCP pathway (Caddy et al., 2010). We

394   previously showed that corneal epithelial cells exhibited slower rates of scratch wound healing when

395   *Vangl2* was inactivated by a tamoxifen-inducible Cre (Findlay et al. 2016). To determine whether the

396   Vangl2-deficient model employed in this study showed a similar defect, monolayers of *Le-Cre*$^{Tg/-}$

397   *Vangl2*$^{fl/fl}$, *Le-Cre*$^{Tg/-}$ *Vangl2*$^{fl/+}$ and *Le-Cre*$^{-/-}$ *Vangl2*$^{fl/fl}$ corneal epithelial cells were cultured as

398   previously described (Leiper et al. 2006) and scratch-wound assays were performed. *Vangl2*–null *Le-*

399   *Cre*$^{Tg/-}$ *Vangl2*$^{fl/fl}$ cells healed significantly more slowly (26.2 ± 3.5 μm/h – mean ± s.e.m.; n = 7) than

400   *Le-Cre*$^{Tg/-}$ *Vangl2*$^{fl/+}$ controls (39.4 ± 3.7 μm/h; n = 9) (Figure 7A). These data confirmed a role for

401   *Vangl2* in the migration during wound healing of corneal epithelial cells.

402   It was considered possible in light of data presented above that the migration defect shown by

403   Vangl2-mutant corneal epithelial cells arises not through a classic PCP pathway but as a secondary

404   consequence of apical-basal defects through a non-PCP mechanism. This was tested by knocking

405   down VANGL2 by siRNA in human corneal epithelial cells in vitro and comparing planar migration of

406   individual isolated cells to that of confluent cells after exposure to a physiological electric field of

407   200 mV/mm that produces robust planar migration towards the cathode (Soong et al. 1990; Zhao et

408   al. 1996; Farboud et al. 2000; Findlay et al. 2016). Classic PCP activity requires cell-cell contact so any

409   effect of VANGL2 knockdown on isolated cells in vitro must represent a non-PCP mechanism of

410   action ~~e.g. through cell adhesion defects~~. Human corneal epithelial cells were transfected with a

411 validated siRNA that causes knockdown of VANGL2 to about 30% of normal levels and which we

412 showed previously causes a significant reduction in cells' ability to migrate cathodally in an applied

413 electric field (Findlay et al. 2016). Control cells were transfected with a negative control nonsense

414 siRNA. Planar migration in an applied electric field was quantified as the Forward Migration Index

415 (FMIX) representing the mean cosine of the angle θ of each cell's direction of travel towards the

416 cathode, with FMIX = -1 representing perfect cathodal migration and FMIX = 0 representing mean

417 random migration (see Methods section). It was found that there was no significant different

418 difference between the behaviour of isolated individual cells compared to that of cells in confluent

419 sheets (Figure 7B). The fact that planar migration was retarded in VANGL2-knockdown cells even in

420 absence of cell-cell contact shows that a classic PCP mechanism was not involved. It suggests that

421 VANGL2 has a non-PCP function, ~~perhaps for normal cell adhesion~~ associated with apical-basal

422 polarity, which leads to migration defects in absence of normal VANGL2 dosage.

423

424

425   **Discussion**

426   **Disrupted stratification of the Vangl2-deficient corneal epithelium.**

427   In this study, the core PCP gene, *Vangl2*, was genetically disrupted in the corneal epithelium and a

428   previously unsuspected role in apical-basal patterning was identified. The stratification of the

429   epithelium was delayed in neonates and badly disrupted in adult mice, with a disorganised

430   arrangement of cells and partial loss of the epithelial basement membrane. Basement membrane

431   defects were shown by light microscopy, immunohistochemistry and transmission electron

432   microscopy. Immunohistochemical and TUNEL analysis showed that while the apical-basal polarity

433   of the individual basal epithelial cells was disrupted (demonstrated by mislocalisation of Scribble

434   protein to the basal edge of basal cells) and cellular morphology was abnormal, the apical or basal

435   identity of cells was maintained in mutant epithelia. Hence proliferation was restricted to the basal

436   layer and apoptosis to the superficial layer of the mutant epithelium. Mutant corneal epithelial cells

437   showed a defect in corneal epithelium wound healing, but this may be secondary to the disruption

438   of the basement membrane.

439

440   The role of PCP pathway proteins in adult vertebrate tissues is poorly known. Whereas classically,

441   the PCP pathway controls the behaviour of epithelial cells in the plane of their basement membrane

442   during embryological development, examples of PCP genes controlling apical-basal behaviour of

443   epithelial cells also exist. For example the uterine epithelium of *Vangl2$^{Lp/Lp}$* mutant mouse embryos

444   is disrupted with loss of apical-basal polarity of columnar epithelial cell (Vandenberg and Sassoon,

445   2009). The columnar epithelium of *Vangl2$^{Lp/Lp}$* mutant uteri at E18.5 is composed of multiple cell

446   layers rather than a single monolayer of columnar epithelial cells, reminiscent of the phenotype in

447   *Vangl2*-null corneal epithelia. Similar findings of apical-basal disruption of epithelia in *Vangl2*

448   mutants were reported by Yates et al. (2010): airway lumina of the lungs of *Vangl2$^{Lp/Lp}$* homozygotes

449   at E14.5 were found to be surrounded by disrupted epithelium. In wild-type lung sections, airway

450   lumina are surrounded by a single layer of epithelium made up of aligned and organized cells. In

451   contrast, in the lungs of *Vangl2$^{Lp/Lp}$* homozygotes the lumina are demarcated by multi-stratified,

452   disorganized epithelial cells that are not aligned uniformly (Yates et al. 2010). Dysregulation or loss

453   of Vangl2 and PCP activity have been shown to mediate increase of matrix metalloprotease activity,

454   loss of epithelial morphology and metastasis in some cancers, a phenotype consistent with the

455   epithelial disruption in *Le-Cre$^{Tg/+}$ Vangl2$^{fl/fl}$* corneas (Cantrell & Jessen 2009; Puvirajesinghe et al.

456   2016).

457   The basement membrane is an extracellular matrix (ECM) composed of secretions from the

458   overlying basal layer of epithelial cells, the basal lamina, and reticular connective tissue (Paulsson,

459   1992; LeBleu et al. 2007). It was thin and, in patches, absent in *Le-Cre*$^{Tg/+}$ *Vangl2*$^{fl/fl}$ mutant eyes.

460   Basement membrane laminin has been shown to secondarily maintain polarisation in epithelial cells

461   (Klein et al. 1988; Xu et al. 2010). PI3K has previously been shown to locate to the basal side of

462   mouse mammary epithelial cells due the influence of laminin in the ECM inducing apical-basal

463   polarity within the cells (Xu et al. 2010). The results obtained in this study suggest that when *Vangl2*

464   expression is lost within corneal epithelial cells they lose polarity and exhibit defects in secretion of

465   basal lamina components from the basal side of cells. The basement membrane is known to be

466   essential for providing chemical cues that aid in epithelial migration (Abrams et al. 2000; Teixeira et

467   al. 2003, 2006). Its absence could be the source of the disorganisation and wound healing delay

468   observed in the *Le-Cre*$^{Tg/+}$ *Vangl2*$^{fl/fl}$ mutant eyes.

469   A reduction in cell adhesion may underlie reduced planar migration of Vangl2-deficient cells in

470   response to wounding or an applied electric field. ~~It is also possible that cell adhesion is~~

471   ~~compromised in *Vangl2*-deficient corneal epithelia.~~ For example, Oteiza et al. (2010) reported

472   impaired cell adhesion linked to planar cell polarity dysfunction: inhibition of *Wnt11* and *Prickle-1a*

473   in Zebrafish impaired cell-cell adhesion of the progenitor cells of Kupffer's vesicle. A direct assay of

474   cell adhesion in conditional knockout cells using single-cell force spectroscopy (Puech et al. 2006)

475   would be informative in this respect.

476   Apical-basal complexes have previously been shown to interact with PCP components (Djiane et al.

477   2005; Dollar et al. 2005; Mahaffey et al. 2013). Vangl2 and Scribble have been linked in the

478   determination of planar polarity in mice: *Scribble*$^{Crc/+}$ *Vangl2*$^{Lp/+}$ double mutants exhibit cochlear

479   disorganisation comparable to that observed in *Vangl2*$^{Lp/Lp}$ mutants (Montcouquiol et al. 2003). The

480   localisation of Scribble along the apical-lateral edge of the epithelial cell layer in control corneal

481   epithelia is consistent with previous observations that Scribble localises with the tight junction

482   protein ZO-1 (Nakagawa & Huibregtse, 2000). The results obtained in this study showed partial

483   mislocalisation of Scribble to the basal side of the innermost layer of the epithelium in *Le-Cre*$^{Tg/-}$

484   *Vangl2*$^{fl/fl}$ mice. This is in contrast to observations made in Drosophila by Courbard et al. (2009) who

485   found no defect in the localisation of Scribble in either *Vangl* or *Frizzled* mutants; they also found

486   that there were no differences in Vangl localisation in Scribble mutants. Yates et al. (2012) observed

487   that *Vangl2*$^{Lp/Lp}$ mutants exhibited no defects in Scribble localisation within the mammalian lung.

488   The data from this study would therefore suggest that the molecular roles of Vangl2 may differ in

489   different tissues.

490 This study has confirmed a novel, sustained role for the core PCP component, Vangl2, in generation

491 and maintenance of stratified epithelial morphology in an adult vertebrate system. It also provides

492 preliminary evidence that at least some of the planar defects observed arise through a non-PCP

493 mechanism, with loss or disruption of the normal epithelial basement membrane. We consider it

494 possible that some or even all of the planar defects may be secondary to a primary failure of apical-

495 basal polarity in the epithelial cells. This may represent a more general model for how PCP signalling

496 is effected in other systems, and warrants further investigation.

497 We previously showed (Dorà et al. 2014) that the *Le-Cre* transgene itself imposes a phenotype on

498 the mouse eye, independently of the presence or absence of floxed alleles of any gene. The

499 phenotype varies in severity with genetic background, but *Le-Cre$^{Tg/-}$* mouse have a tendency to

500 microphthalmia, small disorganised lenses and irido-corneal adhesion with small pupillary opening,

501 though their corneal structure is normal (Dorà et al. 2014). During this study, *Le-Cre$^{Tg/-}$* mice had mild

502 microphthalmia (Fig. 4A) and variable lens fibre disruption. For this reason, all controls in this study

503 were *Le-Cre$^{Tg/-}$*, and significant effects of Vangl2 reported here only for comparison of *Le-Cre$^{Tg/-}$*

504 *Vangl2$^{fl/fl}$* compared to *Le-Cre$^{Tg/-}$ Vangl2$^{fl/+}$* and/or *Le-Cre$^{Tg/-}$ Vangl2$^{+/+}$*. We conclude, in agreement

505 with previous work (Dorà et al. 2014), that *Cre*-negative mice are not valid controls for studies that

506 have used *Le-Cre* to conditionally inactivate floxed genes in the corneal epithelium. Several previous

507 studies have however used the *Le-Cre* transgene to knock out floxed genes in adult eyes and claimed

508 the subsequent defects including microphthalmia, disorganised small lenses or small pupillary

509 openings were due to the conditionally knocked out gene and not the *Le-Cre* transgene itself. Table

510 1 lists these studies. With one exception all have used *Le-Cre* negative mice as controls and have

511 detailed morphological defects in *Le-Cre*-positive *fl/fl* mice that are consistent with the phenotype

512 caused by the *Le-Cre* transgene expression within the developing eye. A few studies also highlight

513 the loss of endogenous *Pax6* expression within the *Le-Cre$^{Tg/-}$* mutant cells but claim the cause is the

514 knocked out gene, whereas Dorà et al. (2014) showed that the eye phenotype in *Le-Cre$^{Tg/-}$* mice was

515 most likely caused by loss of Pax6. In all of these studies it is possible that the phenotype attributed

516 to the gene knockout was in fact, at least in part, caused by the *Le-Cre* transgene and we would

517 suggest that the datasets as a whole should be interpreted in this light.

518

519

525

Author contributions

527   DAP and ASF both performed experiments, analysed data and contributed equally to writing the

528   manuscript. RvL performed experiments and contributed to writing the manuscript. JMC conceived

529   the study, performed experiments and wrote the manuscript.

530

531   **REFERENCES**

532   Abrams G, Schaus S, Goodman, S, et al. (2000) Nanoscale topography of the corneal epithelial basement
533   membrane and Descemet's membrane of the human. *Cornea* **19**, 57-64.

534   Adams DJ, van der Weyden L, (2001) Are we creating problems? Negative effects of Cre recombinase. *Genesis*
535   **29,** 115-115.

536   Ashery-Padan R, Marquardt T, Zhou X, et al. (2000) Pax6 activity in the lens primordium is required for lens
537   formation and for correct placement of a single retina in the eye. *Genes Dev* **14**, 2701-2711.

538   Bilder D, Perrimon N, (2000) Localization of apical epithelial determinants by the basolateral PDZ protein
539   Scribble. *Nature* **403**, 676-680.

540   Buck RC, (1982) Hemidesmosomes of normal and regenerating mouse corneal epithelium. *Virchows Arch B Cell*
541   *Pathol Incl Mol Pathol* **141,** 1-16.

542   Caddy J, Wilanowski T, Darido C, et al. (2010) Epidermal wound repair is regulated by the planar cell
543   polarity signaling pathway. *Dev Cell* **19**, 138–147.

544   Cantrell VA, Jessen JR, (2010) The planar cell polarity protein Van Gogh-Like 2 regulates tumor cell migration
545   and matrix metalloproteinase-dependent invasion. *Cancer Lett* **287**, 54-61.

546   Chen Y, Carlson EC, Chen Z, et al. (2009) Conditional deletion of Cited2 results in defective corneal epithelial
547   morphogenesis and maintenance. *Dev Biol* **334**, 243-252.

548   Chen B, Mao L, Zhang FL, et al. (2013) Loop-tail phenotype in heterozygous mice and neural tube defects in
549   homozygous mice result from a nonsense mutation in the Vangl2 gene. *Genet Mol Res* **12**, 3157-3165.
550

551   Choi JJ, Ting C, Troglic L, et al. (2014) A Role for Smoothened during Murine Lens and Cornea Development.
552   *PLoS One* **9**, e108037.

553   Collinson J.M, Morris L, Reid AI, et al. (2002). Clonal analysis of patterns of growth, stem cell activity, and cell
554   movement during the development and maintenance of the murine corneal epithelium. *Dev Dyn* **224**, 432-
555   440.

556   Cotsarelis G, Cheng S, Dong G, et al. (1989) Existence of slow-cycling limbal epithelial basal cells that can be
557   preferentially stimulated to proliferate: implications on epithelial stem cells. *Cell* **57**, 201-209.

558   Courbard J-R, Djiane A, Wu J, et al. (2009) The apical/basal-polarity determinant Scribble cooperates with the
559   PCP core factor Stbm/Vang and functions as one of its effectors. *Dev Biol* **333**, 67-77.
560
561   Das G, Jenny A., Klein T.J, et al. (2004). Diego interacts with Prickle and Strabismus/Van Gogh to localize planar
562   cell polarity complexes. *Development* **131**, 4467–4476.

563   Devenport D, (2014) The cell biology of planar cell polarity. *J Cell Biol* **207**, 171-179.

564   Di Girolamo N, Bobba S, Raviraj V, et al. (2015) Tracing the fate of limbal epithelial progenitor cells in the
565   murine cornea. *Stem Cells* **33**, 157-169.

566   Djiane A, Yogev S, Mlodzik M, (2005) The Apical Determinants aPKC and dPatj Regulate Frizzled-Dependent
567   Planar Cell Polarity in the *Drosophila* Eye. *Cell* **121**, 621-631.

568   Dollar GL, Weber U, Mlodzik M, et al. (2005) Regulation of Lethal giant larvae by Dishevelled. *Nature* **437**,
569   1376-1380.

570   Dorà NJ, Collinson JM, Hill RE, et al. (2014) Hemizygous Le-Cre Transgenic Mice Have Severe Eye Abnormalities
571   on Some Genetic Backgrounds in the Absence of LoxP Sites. *Plos One,* **9**, e109193.

572   Farbourd B, Nuccitelli R, Schwab IR, et al. (2000) DC electric fields induce rapid directional migration in
573   cultured human corneal epithelial cells. *Exp Eye Res* **70**, 667-673.

574   Forrester JV, Dick AD, Mcmenamin PG, et al. (2001) *The Eye. Basic Science in Practice* Saunders: Edinburgh.

575   Gao, B, Song H, Bishop K, et al. (2011) Wnt signaling gradients establish planar cell polarity by inducing Vangl2
576   phosphorylation through Ror2. *Dev Cell* **20**,163-176.

577   Goto T, Keller R, (2002) The Planar Cell Polarity Gene *Strabismus* Regulates Convergence and Extension and
578   Neural Fold Closure in *Xenopus*. *Dev Biol* **247**, 165-181.

579   Greene ND, Girrelli D, van Straaten, et al. (1998) Abnormalities of floor plate, notochord and somite
580   differentiation in the loop-tail (Lp) mouse: a model of severe neural tube defects. *Mech Dev* **73,** 59-72.

581   Gu H, Marth JD, Orban PC, et al. (1994) Deletion of a DNA polymerase beta gene segment in T cells using cell
582   type-specific gene targeting. *Science,* **265**, 103-106.

583   Gupta D, Harvey SA, Kenchgowda D, et al. (2013) Regulation of mouse lens maturation and gene expression by
584   Krüppel-like factor 4. *Exp Eye Res* **116**, 205-218.

585   Harris BZ, Lim WA, (2001) Mechanism and role of PDZ domains in signaling complex assembly. *J Cell Science*
586   **114**, 3219-3231.

587   Henderson DJ, Conway SJ, Greene ND, et al. (2001) Cardiovascular defects associated with abnormalities in
588   midline development in the Loop-tail mouse mutant. *Circ Res* **89**, 6-12.

589   Henriksson JT, McDermott AM, Bergmanson JP, (2009) Dimensions and morphology of the cornea in three
590   strains of mice. *Invest Ophthalmol Vis Sci* **50**, 3648-3654.

591   Jia J, Lin M, Zhang L, et al. (2007) The Notch signaling pathway controls the size of the ocular lens by directly
592   suppressing p57Kip2 expression. *Molec Cell Biol* **27**, 7236-7247.

593   Joo JH, Kim YH, Dunn NW, et al. (2010) Disruption of mouse corneal epithelial differentiation by conditional
594   inactivation of pnn. *Invest Ophthalmol Vis Sci* **51**, 1927-1934.

595   Kenchegowda, D., Swamynathan S, Gupta D, et al. (2011) Conditional disruption of mouse Klf5 results in
596   defective eyelids with malformed meibomian glands, abnormal cornea and loss of conjunctival goblet cells.
597   *Dev Biol* **356**, 5-18.

598   Kibar Z, Vogan K.J, Groulx N, et al. (2001) Ltap, a mammalian homolog of Drosophila Strabismus/Van Gogh, is
599   altered in the mouse neural tube mutant Loop-tail. *Nat Genet* **28**, 251-255.

600   Klein G, Langegger M, Timpl R, (1988) Role of laminin A chain in the development of epithelial cell polarity. *Cell*
601   **55**, 331-341.

602   Kumichel A, Knust E, (2014) Apical localisation of crumbs in the boundary cells of the *Drosophila* hindgut Is
603   independent of its canonical interaction partner stardust. *PLoS ONE* **9**, e94038.

604   Le TT, Conley KW, Brown NL, (2009) Jagged 1 is necessary for normal mouse lens formation. *Dev Biol* **328**, 118-
605   126.

606   LeBleu VS, Macdonald B, Kalluri R, (2007) Structure and function of basement membranes. *Exp Biol Med* **232**,
607   1121-1129.

608   Lehrer MS, Sun TT, Lavker RM, (1998) Strategies of epithelial repair: modulation of stem cell and transit
609   amplifying cell proliferation. *J Cell Sci* **111,** 2867-2875.

610   Lei Y, Zhang T, Li H, et al. (2010) VANGL2 mutations in human cranial neural-tube defects. *N Engl J Med* **362**,
611   2232-2235.

612   Li H, Tao C, Cai Z, et al. (2014) Frs2alpha and Shp2 signal independently of Gab to mediate FGF signaling in lens
613   development. *J Cell Sci,* **127**, 571-582.

614   Li HF, Petroll WM, Møller-Pederson T et al. (1997) Epithelial and corneal thickness measurements by in vivo
615   confocal microscopy through focusing (CMTF). *Curr Eye Res* **16,** 214-221.

616   Lin D, Edwards AS, Fawcett JP, et al. (2000) A mammalian Par-3-Par-6 complex implicated in CdC42/Rac1 and
617   aPKC signalling and cell polarity. *Nat Cell Biol* **2**, 540–547.

618   Liu W, Lagutin OV, Mende M, et al. (2006) Six3 activation of Pax6 expression is essential for mammalian lens
619   induction and specification. *EMBO J* **25**, 5383-5395.

620   Lu X, Borchers AG, Jolicoeur C, et al. (2004) PTK7/CCK-4 is a novel regulator of planar cell polarity in
621   vertebrates. *Nature* **430**, 93-98.

622   Mao Y, Mulvaney J, Zakaria S, et al. (2011) Characterization of a Dchs1 mutant mouse reveals requirements for
623   Dchs1-Fat4 signaling during mammalian development. *Development* **138**, 947-957.

624   Mahaffey JP, Grego-Bessa J, Liem KF et al. (2013) Cofilin and Vangl2 cooperate in the initiation of planar cell
625   polarity in the mouse embryo. *Development* **140**, 1262-1271.

626   Montcouquiol M, Rachel RA, Lanford PJ, et al. (2003) Identification of Vangl2 and Scrb1 as planar polarity
627   genes in mammals. *Nature* **423**, 173-177.

628   Montcouquiol M, Sans N, Huss D, et al. (2006) Asymmetric localization of Vangl2 and Fz3 indicate novel
629   mechanisms for planar cell polarity in mammals. *J Neurosci* **26**, 5265-5275.

630   Mort RL, Douvaras P, Morley SD, Dorà, NJ et al. (2012) Stem cells and corneal epithelial maintenance: insights
631   from the mouse and other animal models. *Results Probl Cell Differ* **55**, 357-94

632   Murdoch JN, Doudney K, Paternotte C, et al. (2001) Severe neural tube defects in the loop-tail mouse result
633   from mutation of Lpp1, a novel gene involved in floor plate specification. Hum Molec Genet **10**, 2593-2601.

634   Nagasaki T, Zhao J, (2003) Centripetal movement of corneal epithelial cells in the normal adult mouse. *Invest
635   Ophthalmol Vis Sci* **44**, 558-566.

636   Nakgawa S, Huibregtse JM, (2000) Human scribble (Vartul) is targeted for ubiquitin-mediated degradation by
637   the high-risk papillomavirus E6 proteins and the E6AP ubiquitin-protein ligase. *Molec Cell Biol* **20**, 8244-8253.

638 Notara M, Daniels JT, (2010) Characterisation and functional features of a spontaneously immortalised human
639 corneal epithelial cell line with progenitor-like characteristics. *Brain Res Bull* **81**, 279-286.

640 Nguyen MM, Rivera C, Griep AE, (2005) Localization of PDZ domain containing proteins Discs Large-1 and
641 Scribble in the mouse eye. *Molec Vis* **11**, 1183-1199.

642 Oteiza P, Koppen M, Krieg M, et al. (2010). Planar cell polarity signalling regulates cell adhesion properties in
643 progenitors of the zebrafish laterality organ. *Development* **137**, 3459-3468.

644 Park M, Moon RT, (2001) The planar cell-polarity gene stbm regulates cell behaviour and cell fate in vertebrate
645 embryos. *Nat Cell Biol* **4**, 20-25.

646 Paulsson M, (1992) Basement membrane proteins: structure, assembly, and cellular interactions. *Crit Rev
647 Biochem Mol Biol* **27**: 93-127.

648 Phillips HM, Murdoch JN, Chaudhry B, et al. (2005) Vangl2 acts via RhoA signaling to regulate polarized cell
649 movements during development of the proximal outflow tract. *Circ Res* **96**, 292-299.

650 Puech PH, Poole K, Knebel D, Muller DJ, (2006) A new technical approach to quantify cell-cell adhesion forces
651 by AFM. *Ultramicroscopy* **106**, 637-644.

652 Puvirajesinghe TM, Bertucci F, Jain A, et al. (2016) Identification of p62/SQSTM1 as a component of non-
653 canonical wnt VANGL2-JNK signalling in breast cancer. *Nat Commun* **7**, 10318.

654 Ramaesh T, Collinson JM, Ramaesh K, et al. (2003). Corneal abnormalities in *Pax6*$^{+/-}$ small eye mice mimic
655 human aniridia-related keratopathy. *Invest Ophthalmol Vis Sci* **44**, 1871-1878.

656 Ramsbottom SA, Sharma V, Rhee HJ, et al. (2014) Vangl2-regulated polarisation of second heart field-derived
657 cells is required for outflow tract lengthening during cardiac development. *PLoS Genetics* **10**, e1004871.

658 Rajnicek AM, Foubister LE, McCaig CD, (2006) Growth cone steering by a physiological electric field requires
659 dynamic microtubules, microfilaments and Rac-mediated filopodial asymmetry. *J Cell Sci* **119**, 1736-1745.

660 Ren H, Wilson, G, (1996) Apoptosis in the corneal epithelium. *Invest Ophthalmol Vis Sci* **37**, 1017-1025.

661 Rodriguez-Boulan, E. and Macara, I. G. (2014). Organization and execution of the epithelial polarity
662 programme. *Nat Rev Molec Cell Biol* **15**, 225–242

663 Roszko I, Sawada A, Solnica-Krezel L, (2009) Regulation of convergence and extension movements during
664 vertebrate gastrulation by the Wnt/PCP pathway. *Sem Cell Dev Biol* **20**, 986-997.

665 Rowan S, Conley KW, Le TT, et al., (2008). *Notch* signaling regulates growth and differentiation in the
666 mammalian lens. *Dev Biol* **321**, 111-122.

667 Saravanamuthu SS, Le TT, Gao CY, et al. (2012) Conditional ablation of the Notch2 receptor in the ocular lens.
668 *Dev Biol* **362**, 219-229.

669 Smith RS, Sundberg JP, John SW, (2001) The anterior segment and ocular adnexae. in *Systematic Evaluation of
670 the Mouse Eye: Anatomy, Pathology and Biomethods. Eds: Smith RS, John SWM, Nishina PM* et al. *CRC Press,
671 Boca Raton, FL.*

672 Soong HK, Parkinson WC, Bafna S, et al. (1990) Movements of cultured corneal epithelial cells and stromal
673 fibroblasts in electric fields. *Invest Ophthalmol Vis Sci* **31**, 2278-2282.

674 Strong LC, Hollander WF, (1949) Hereditary loop-tail in the house mouse accompanied by imperforate vagina
675 and with lethal craniorachischisis when homozygous. *J Hered* **40**, 329-344.

676 Taylor J, Abramova N, Charlton J, et al. (1998. Van Gogh: a new Drosophila tissue polarity gene. *Genetics* **150**,
677 199-210.

678 Teixeira AI, McKie GA, Foley JD, et al. (2006) The effect of environmental factors on the response of human
679 corneal epithelial cells to nanoscale substrate topography. *Biomaterials* 27, 3945-3954.

680 Teixeira AI, Abrams GA, Bertics PJ, et al. (2003) Epithelial contact guidance on well-defined micro- and
681 nanostructured substrates. *J Cell Sci* **116**, 1881-1892.

682 Thoft RA, Friend J, (1983) The X, Y, Z hypothesis of corneal epithelial maintenance. *Invest Ophthalmol Vis Sci*
683 **24**, 1442-1443.

684 Vandenberg AL, Sassoon DA, (2009) Non-canonical Wnt signaling regulates cell polarity in female reproductive
685 tract development via van gogh-like 2. *Development* **136**, 1559-1570.

686 Wallingford JB, (2012) Planar cell polarity and the developmental control of cell behavior in vertebrate
687 embryos. *Annu Rev Cell Dev Biol* **28** 627-653.

688 Wansleeben C, Meijlink F, (2011) The planar cell polarity pathway in vertebrate development. *Dev Dyn* **240**,
689 616-626.

690 Whiteman EL, Fan S, Harder JL, et al. (2014) Crumbs3 is essential for proper epithelial development and
691 viability. *Mol Cell Biol* **34**, 43–56.

692 Williams S, Altmann CR, Chow RL, et al. (1998) A highly conserved lens transcriptional control element from
693 the Pax-6 gene. *Mech Dev* **73**, 225-229.

694 Xiao Z, Patrakka J, Nukui M, et al. (2011) Deficiency in Crumbs homolog 2 (Crb2) affects gastrulation and
695 results in embryonic lethality in mice. *Dev Dyn* **240**, 2646–2656.

696 Xu R, Spencer VA, Groesser DL, et al. (2010). Laminin regulates PI3K basal localization and activation to sustain
697 STAT5 activation. *Cell Cycle* **9**, 4315-4322.

698 Yamben IF, Rachel RA, Shatadal S, et al. (2013) Scrib is required for epithelial cell identity and prevents
699 epithelial to mesenchymal transition in the mouse. *Dev Biol* **384**, 41-52.

700 Yates LL, Schnatwinkel C, Murdoch JN, et al. (2010) The PCP genes Celsr1 and Vangl2 are required for normal
701 lung branching morphogenesis. *Hum. Mol. Gen.,* **19**, 2251-2267.

702 Yates LL, Schnatwinkel C, Hazelwood L, et al. (2013) Scribble is required for normal epithelial cell–cell contacts
703 and lumen morphogenesis in the mammalian lung. *Dev Biol* **373**, 267-280.

704 Yi X, Wang Y, Yu FS, (2000) Corneal epithelial tight junctions and their response to lipopolysaccharide
705 challenge. *Invest Ophthalmol Vis Sci* **41**. 4093-4100.
706
707 Yin H, Copley CO, Goodrich LV, Deans MR (2012) Comparison of phenotypes between different *vangl2* mutants
708 demonstrates dominant effects of the Looptail mutation during hair cell development. PLoS ONE 7(2): e31988.

709

710 Zhang Y, Yeh LK, Zhang S, et al. (2015) Wnt/β-catenin signaling modulates corneal epithelium stratification via
711 inhibition of Bmp4 during mouse development. *Development* **142**, 3383-3393.

712 Zhang J, Upadhya D, Lu L, et al. (2015) Fibroblast growth factor receptor 2 (FGFR2) is required for corneal
713 epithelial cell proliferation and differentiation during embryonic development. *PloS One* **10**, e0117089.

714 Zhao M, Agius-Fernandez A., Forrester JV, et al. (1996) Directed migration of corneal epithelial sheets in
715 physiological electric fields. *Invest Ophthalmol Vis Sci* **37**, 2548-2558.

716 Zhao Q, Zhao J-Y, Wu D, et al. (2012). Mutually inductive interactions between the lens and retina require ALK3
717 functions during mouse embryonic development. *Int J Ophthalmol* **5**, 119-124.

718 Zhao Q, Zhao J-Y, Zhang J-S, (2015) Influence of bone morphogenetic protein type IA receptor conditional
719 knockout in lens on expression of bone morphogenetic protein 4 in lens. *Int J Ophthalmol* **8**, 57-60.

720 Zhao M, Song B, Pu J, et al. (2006) Electrical signals control wound healing through phosphatidylinositol-3-OH
721 kinase-γ and PTEN. *Nature* **442**, 457-460.

722 Zieske JD, (2004) Corneal development associated with eyelid opening. *Int J Dev Biol* **48**, 903-911.

723

724

725

726

727   **TABLE 1. STUDIES THAT HAVE USED LE-CRE MICE TO STUDY EYE DEVELOPMENT**

Publication	Gene	Control	Phenotype Observed
Zhao et al. 2015	*ALK3*	*Le-Cre*^{-/-} mice	Observed a smaller lens in *Le-Cre*[Tg/-] mice
Zhang et al. 2015	*FGFr2*	*Le-Cre*^{-/-} mice	Observed a thinner corneal epithelial layer when compared to wild-type mice, and abnormal Pax6 immunostaining
Choi et al. 2014	*Smoothened*	*Le-Cre*^{-/-} mice	Observed microphthalmia in *Le-Cre*[Tg/-] mice.
Li et al. 2014	*Frs2* and *Shp2*	*Le-Cre*^{-/-} mice	Found that deletion of either gene caused a decrease in lens size.
Yamben et al. 2013	*Scribble*	*Le-Cre*^{-/-} mice	Observed small, misshapen lenses with central opacity in *Le-Cre*[Tg/-] mice.
Gupta et al. 2013	*Klf4*	*Le-Cre*^{-/-} mice	Observed small lens with central opacity in *Le-Cre*[Tg/-] mice.
Zhao et al. 2012	*ALK3*	*Le-Cre*^{-/-} mice	Observed small lens with notable defects in fibre cell differentiation in *Le-Cre*[Tg/-] mice.
Saravanamuthu et al. 2012	*Notch2*	*Le-Cre*^{-/-} mice	Observed microphthalmia, and reduced pupillary openings.
Kenchegowda et al. 2011	*Klf5*	*Le-Cre*^{-/-} mice	Observed microphthalmia and closed eyelids, with small lenses in *Le-Cre*[Tg/-] mice.
Joo et al. 2010	*Pnn*	*Le-Cre*^{-/-} mice	Observed microphthalmia.
Chen et al. 2009	*Cited2*	*Le-Cre*^{-/-} mice	Observed microphthalmia and thin opaque cornea. Found *Le-Cre*[Tg/-] *Cited2*^{fl/fl} mice have a decrease in *Pax6* expression.
Le et al. 2009	*Jagged1*	*Le-Cre*[Tg/-] *Jagged1*^{fl/+} and *Le-Cre*^{-/-} mice	Although this paper compares homozygous conditional knock-outs to their heterozygous counterparts, they still claim all observations – microphthalmia and decreased pupillary openings – are due to a reduced expression of *Jagged1*.
Rowan et al. 2008	*Rbp-J*	*Le-Cre*^{-/-} mice	Microphthalmia, small pupillary opening
Jia et al. 2007	*Rbp-J*	*Le-Cre*^{-/-} mice	Observed microphthalmia and small lens.
Liu et al. 2006	*Six3*	*Le-Cre*^{-/-} mice	Observed lens defects, reduced size, cataracts and absence.

728

729

730

731

732   **FIGURE LEGENDS**

733

734   **FIGURE 1. Corneal epithelial abnormalities in adult *Vangl2*-mutant mice.** Haematoxylin-and eosin

735   staining of tissue sections of adult mice corneas. **(A)** Wild-type cornea showing stratified epithelium

736   sitting on hypocellular collagenous corneal stroma. **(B)** Cornea from *Vangl2$^{Lp/+}$* mouse (littermate of

737   A) with mild disruption to apical-basal organisation of epithelium (arrowhead). **(C-E)** Cornea from *Le-*

738   *Cre$^{Tg/-}$ Vangl2$^{fl/fl}$* mouse (conditional knockout, cKO) showing irregularity of corneal epithelium,

739   disruption to normal stratification, and projection of basal cells into the corneal stroma. Corneal

740   epithelia could be abnormally thin (D) or thick (E) with sharp transitions between the thinner and

741   thicker domains, phenomena never seen in *Le-Cre$^{Tg/-}$ Vangl2$^{fl/+}$* or *Le-Cre$^{-/-}$ Vangl2$^{fl/fl}$* (n > 100)

742   controls. Scale bar represents 50 μm (A-C), 20 μm (D, E).

743

744   **FIGURE 2. Corneal epithelial abnormalities in neonatal *Vangl2*-mutant mice.** (A) At postnatal day 5,

745   the corneal epithelium of *Le-Cre$^{Tg/-}$ Vangl2$^{fl/+}$* control mice is a uniform 2-3 cells thick (n = 6). (B) In

746   contrast, all corneal epithelia of *Le-Cre$^{Tg/-}$ Vangl2$^{fl/+}$* littermates (n = 5) exhibited irregularities of

747   stratification, with the epithelium being 1-2 cells thick and with areas of cytoplasmic covering only.

748   Scale bar represents 20 μm.

749

750   **FIGURE 3. Corneal epithelial basement membrane deficiency in adult *Vangl2*-mutant mice.**

751   Haematoxylin and eosin (H&E) staining (top), and immunohistochemistry for ECM proteins laminin

752   (middle) and collagen IV (bottom) in adult *Le-Cre$^{Tg/-}$ Vangl2$^{fl/+}$* control mice (left) and *Le-Cre$^{Tg/-}$*

753   *Vangl2$^{fl/+}$* littermates (right). Arrows point to the basement membrane. In controls, the basement

754   membrane is visible in H&E-stained controls as a strongly stained lamina immediately underneath

755   the basal surface of the epithelial cells, sitting on a more weakly stained ECM. This is reproducibly

756   not visible or patchy in mutants (right). Laminin and collagen IV staining in mutants is absent or

757   patchy and thin, confirming the light microscopy and Supplementary transmission electron

758   microscopy. DAPI staining (blue) visualises cell nuclei. Scale bar: 40 μm.

759

760   **FIGURE 4. Morphometric analysis of *Vangl2*-mutant corneas.** Corneal epithelial diameter (top) and

761   thickness (bottom) were measured. *Le-Cre*-positive corneas were slightly but very significantly

762   smaller than *Le-Cre*-negative corneas, irrespective of Vangl2 genotype. Conditional knockout of

763   Vangl2 lead to increased mean thickness of the corneal epithelium, both centrally and peripherally,

764   accompanying the cellular, morphological and molecular defects described in this paper.

765

766   **FIGURE 5. Molecular analysis of cell proliferation and apoptosis in Vangl2-mutant corneal**

767   **epithelia**. **(A-C)** TUNEL analysis of apoptotic cell death. In both *Le-Cre*$^{Tg/-}$ *Vangl2*$^{fl/+}$ control corneas

768   (A) and *Le-Cre*$^{Tg/-}$ *Vangl2*$^{fl/fl}$ conditional knockouts (B) apoptosis (green fluorescent labelling) was

769   restricted to the most superficial cell layer, with no apoptotic events noted in any other layer of the

770   corneal epithelium (n = 3 of both genotypes). (C) is a positive control - tissue section digested with

771   DNAse1 to create double-stranded breaks in DNA of all cells). **(D, E).** Immunohistochemical analysis

772   of cell proliferation in corneal epithelium of mice after a single injection of BrdU. In both *Le-Cre*$^{Tg/-}$

773   *Vangl2*$^{fl/+}$ control corneas (E) and *Le-Cre*$^{Tg/-}$ *Vangl2*$^{fl/fl}$ conditional knockouts (F), DNA replication was

774   restricted to the basal layer of the corneal epithelium, with no proliferation events more apically.

775

776   **FIGURE 6. Cell polarity and cell fate markers in corneal epithelia of *Vangl2*-mutants.**

777   Immunohistochemical labelling of Scribble, PI3K, P63, cytokeratin-12 and Pax6 in *Le-Cre*$^{Tg/-}$ *Vangl2*$^{fl/+}$

778   control corneas and *Le-Cre*$^{Tg/-}$ *Vangl2*$^{fl/fl}$ conditional knockouts. Asterisks denote selected *Vangl2*-

779   mutant cells with atypical localisation of Scribble to the basal boundary, suggesting disrupted apical-

780   basal polarity of the basal epithelial cells. PI3K is upregulated in the basal cells of control epithelia

781   but not of Vangl2 knockout cells. Other markers of cell fate and apical-basal identity are expressed

782   normally in mutant epithelia. n = 3-9 for all markers. Scale bar represents 40 µm.


783

784   **FIGURE 7. Planar migration defects in Vangl2-deficient corneal epithelial cells. (A)** Wound healing

785   rate of in vitro cultured adult mouse corneal epithelial cells. The rate of migration of *Le-Cre*$^{Tg/-}$

786   *Vangl2*$^{fl/fl}$ cells following scratch-wounding was significantly slower than that of *Le-Cre*$^{Tg/-}$ *Vangl2*$^{fl/+}$

787   and *Le-Cre*$^{-/-}$ *Vangl2*$^{fl/fl}$ cells. (One-way ANOVA: F = 3.720, *P* = 0.0309). **(B)** Cathodal migration

788   (expressed as forward migration index – FMIX – as described in Materials and Methods), for human

789   corneal epithelial cells after VANGL2 knockdown to ~30% of normal protein levels. The response of

790   cell cultured at low density (individual cells) (light grey) was not significantly different from that of

791   confluent cells (dark grey).

792
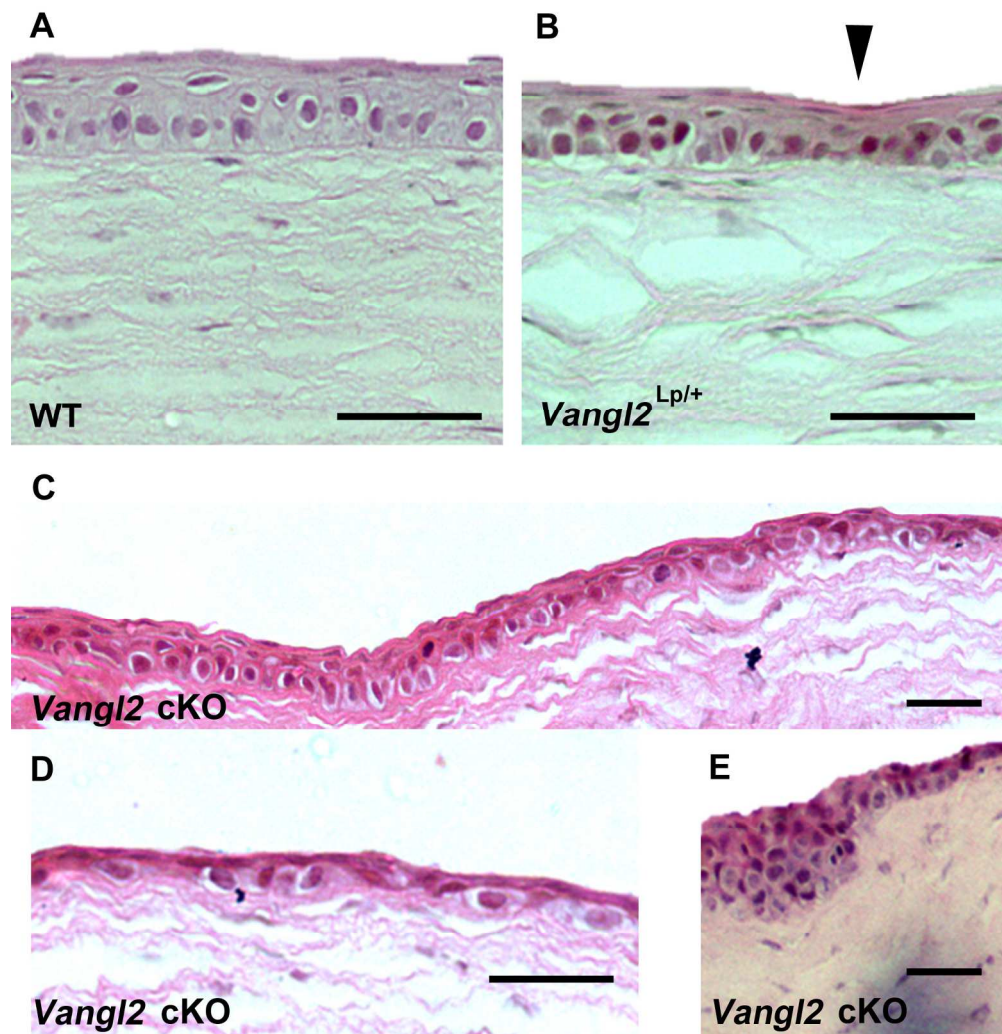
Corneal epithelial abnormalities in adult Vangl2-mutant mice. Haematoxylin-and eosin staining of tissue sections of adult mice corneas. (A) Wild-type cornea showing stratified epithelium sitting on hypocellular collagenous corneal stroma. (B) Cornea from Vangl2Lp/+ mouse (littermate of A) with mild disruption to apical-basal organisation of epithelium (arrowhead). (C-E) Cornea from Le-CreTg/- Vangl2fl/fl mouse (conditional knockout, cKO) showing irregularity of corneal epithelium, disruption to normal stratification, and projection of basal cells into the corneal stroma. Corneal epithelia could be abnormally thin (D) or thick (E) with sharp transitions between the thinner and thicker domains, phenomena never seen in Le-CreTg/- Vangl2fl/+ or Le-Cre-/- Vangl2fl/fl (n>100) controls. Scale bar represents 50 μm (A-C), 20 μm (D, E).

184x193mm (300 x 300 DPI)
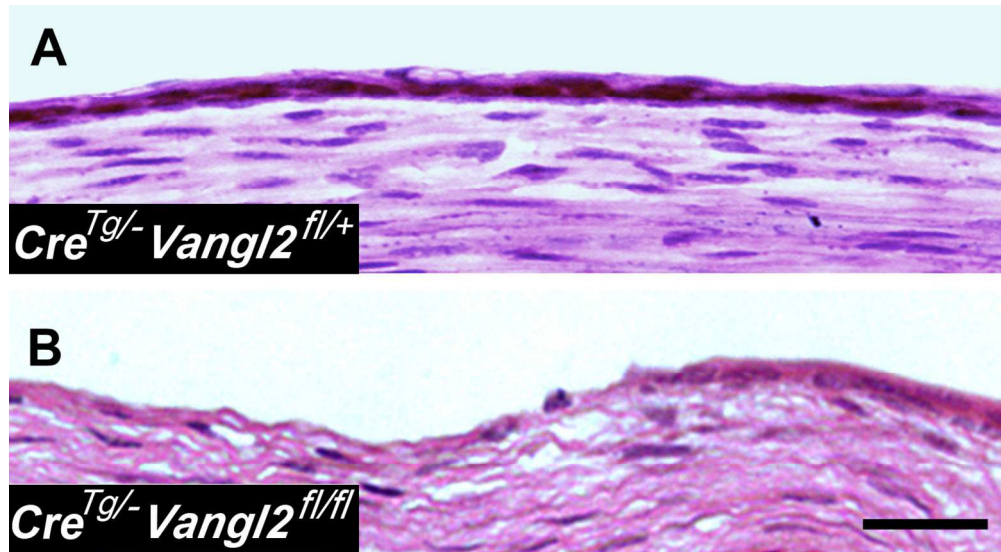
Corneal epithelial abnormalities in neonatal Vangl2-mutant mice. (A) At postnatal day 5, the corneal epithelium of Le-CreTg/- Vangl2fl/+ control mice is a uniform 2-3 cells thick (n = 6). (B) In contrast, all corneal epithelia of Le-CreTg/- Vangl2fl/+ littermates (n = 5) exhibited irregularities of stratification, with the epithelium being 1-2 cells thick and with areas of cytoplasmic covering only. Scale bar represents 20 μm.

124x68mm (300 x 300 DPI)
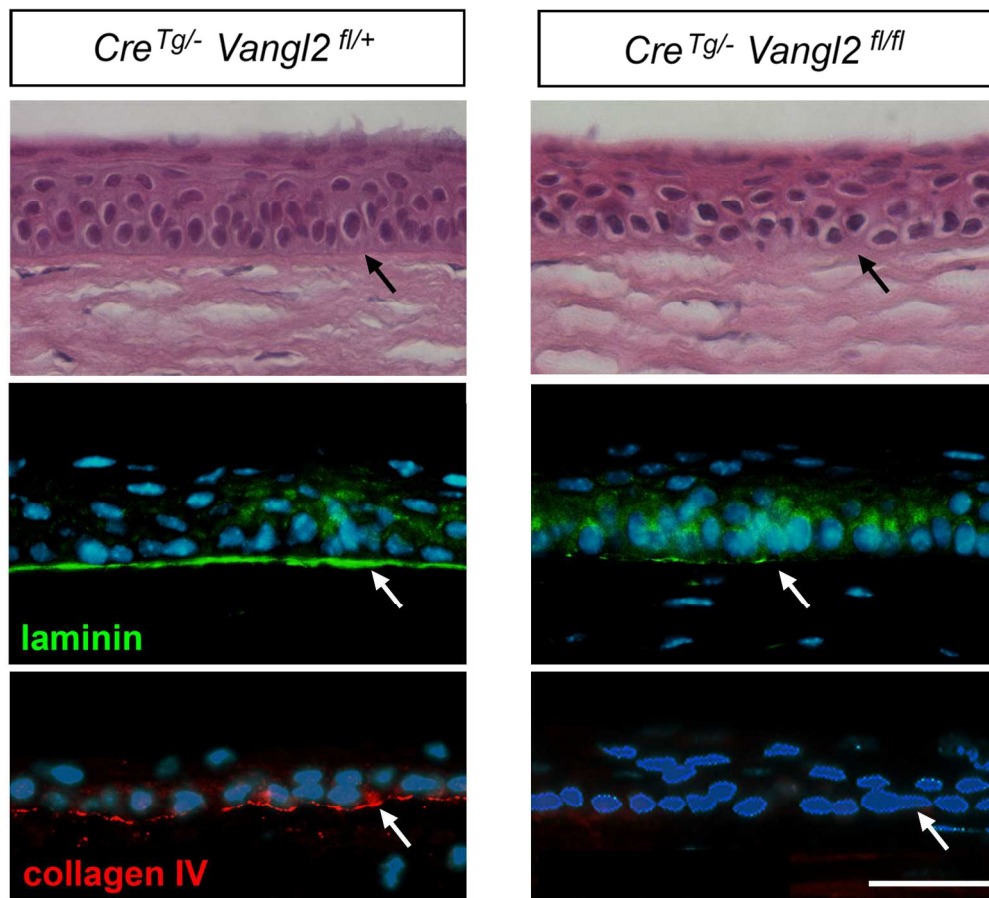
Corneal epithelial basement membrane deficiency in adult Vangl2-mutant mice. Haematoxylin and eosin (H&E) staining (top), and immunohistochemistry for ECM proteins laminin (middle) and collagen IV (bottom) in adult Le-CreTg/- Vangl2fl/+ control mice (left) and Le-CreTg/- Vangl2fl/+ littermates (right). Arrows point to the basement membrane. In controls, the basement membrane is visible in H&E-stained controls as a strongly stained lamina immediately underneath the basal surface of the epithelial cells, sitting on a more weakly stained ECM. This is reproducibly not visible or patchy in mutants (right). Laminin and collagen IV staining in mutants is absent or patchy and thin, confirming the light microscopy and Supplementary transmission electron microscopy. DAPI staining (blue) visualises cell nuclei. Scale bar: 40 μm.

181x164mm (300 x 300 DPI)

A

B

Central   Peripheral

$Cre^{Tg/-}$ $Vangl2^{fl/+}$ ☐

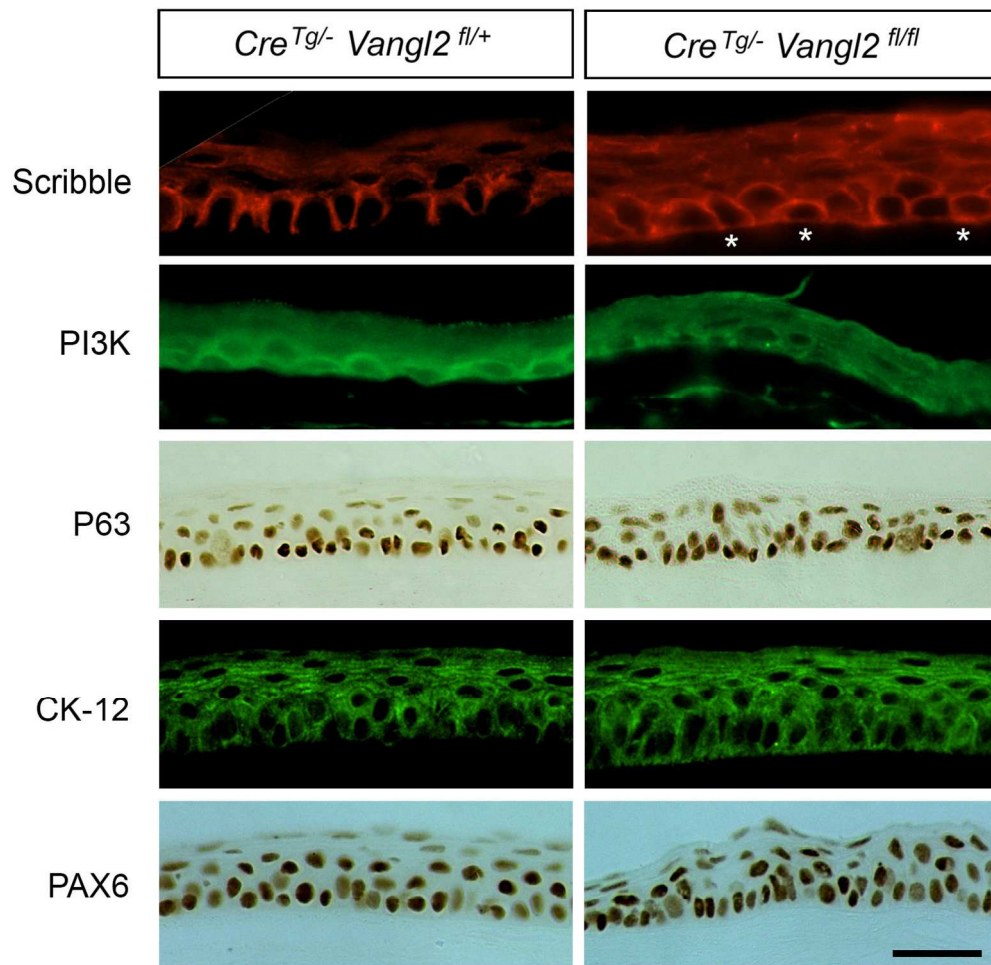$Cre^{Tg/-}$ $Vangl2^{fl/fl}$ ▨

$Cre^{-/-}$ ■
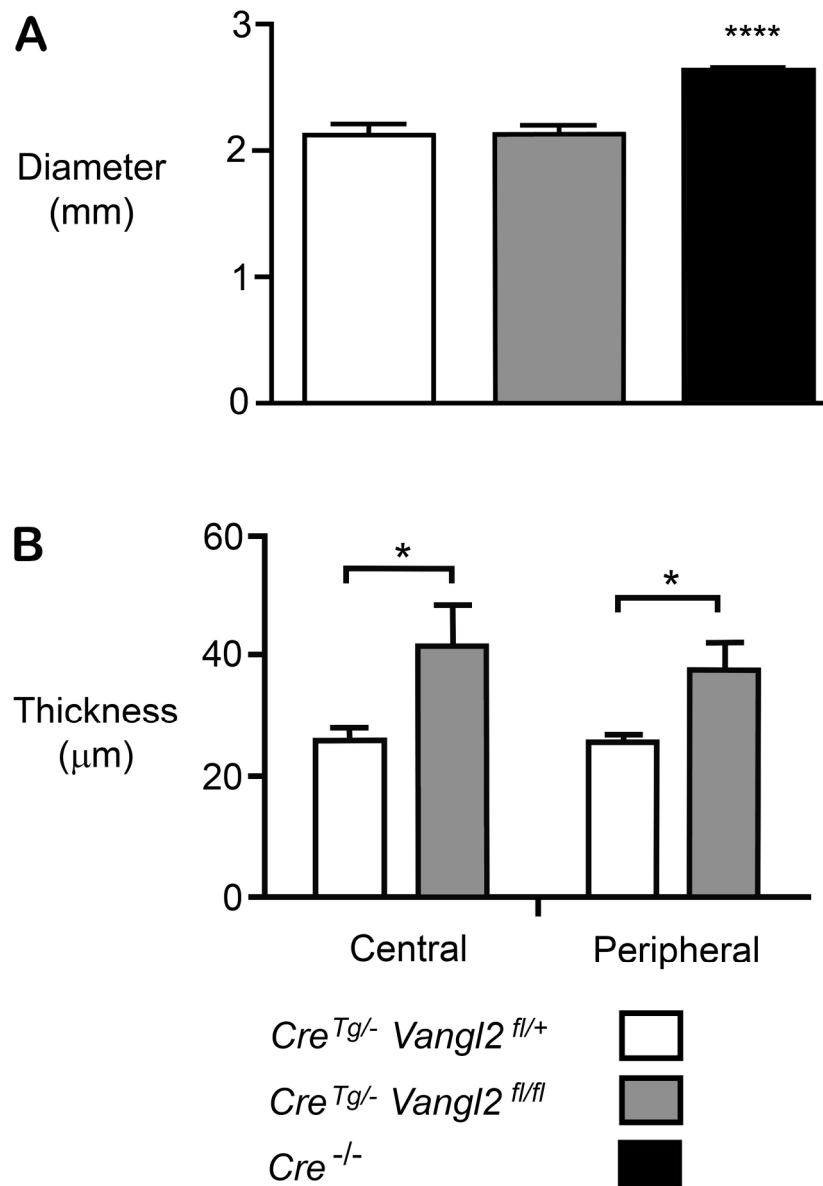
Morphometric analysis of Vangl2-mutant corneas. Corneal epithelial diameter (top) and thickness (bottom) were measured. Le-Cre-positive corneas were slightly but very significantly smaller than Le-Cre-negative corneas, irrespective of Vangl2 genotype. Conditional knockout of Vangl2 lead to increased mean thickness of the corneal epithelium, both centrally and peripherally, accompanying the cellular, morphological and molecular defects described in this paper.

161x232mm (300 x 300 DPI)
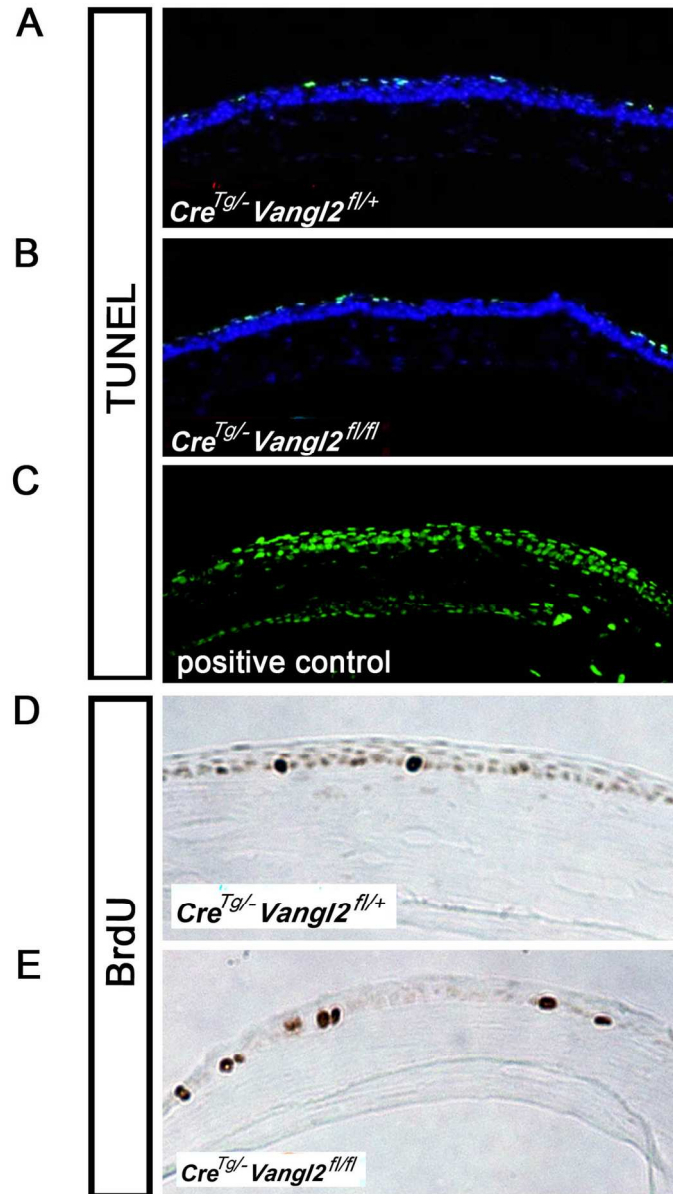
Molecular analysis of cell proliferation and apoptosis in Vangl2-mutant corneal epithelia. (A-C) TUNEL analysis of apoptotic cell death. In both Le-CreTg/- Vangl2fl/+ control corneas (A) and Le-CreTg/- Vangl2fl/fl conditional knockouts (B) apoptosis (green fluorescent labelling) was restricted to the most superficial cell layer, with no apoptotic events noted in any other layer of the corneal epithelium (n = 3 of both genotypes). (C) is a positive control - tissue section digested with DNAse1 to create double-stranded breaks in DNA of all cells). (D, E). Immunohistochemical analysis of cell proliferation in corneal epithelium of mice after a single injection of BrdU. In both Le-CreTg/- Vangl2fl/+ control corneas (E) and Le-CreTg/- Vangl2fl/fl conditional knockouts (F), DNA replication was restricted to the basal layer of the corneal epithelium, with no proliferation events more apically.

124x221mm (300 x 300 DPI)

Cell polarity and cell fate markers in corneal epithelia of Vangl2-mutants. Immunohistochemical labelling of Scribble, PI3K, P63, cytokeratin-12 and Pax6 in Le-CreTg/- Vangl2fl/+ control corneas and Le-CreTg/- Vangl2fl/fl conditional knockouts. Asterisks denote selected Vangl2-mutant cells with atypical localisation of Scribble to the basal boundary, suggesting disrupted apical-basal polarity of the basal epithelial cells. PI3K is upregulated in the basal cells of control epithelia but not of Vangl2 knockout cells. Other markers of cell fate and apical-basal identity are expressed normally in mutant epithelia. n = 3-9 for all markers. Scale bar represents 40 μm.

148x148mm (300 x 300 DPI)
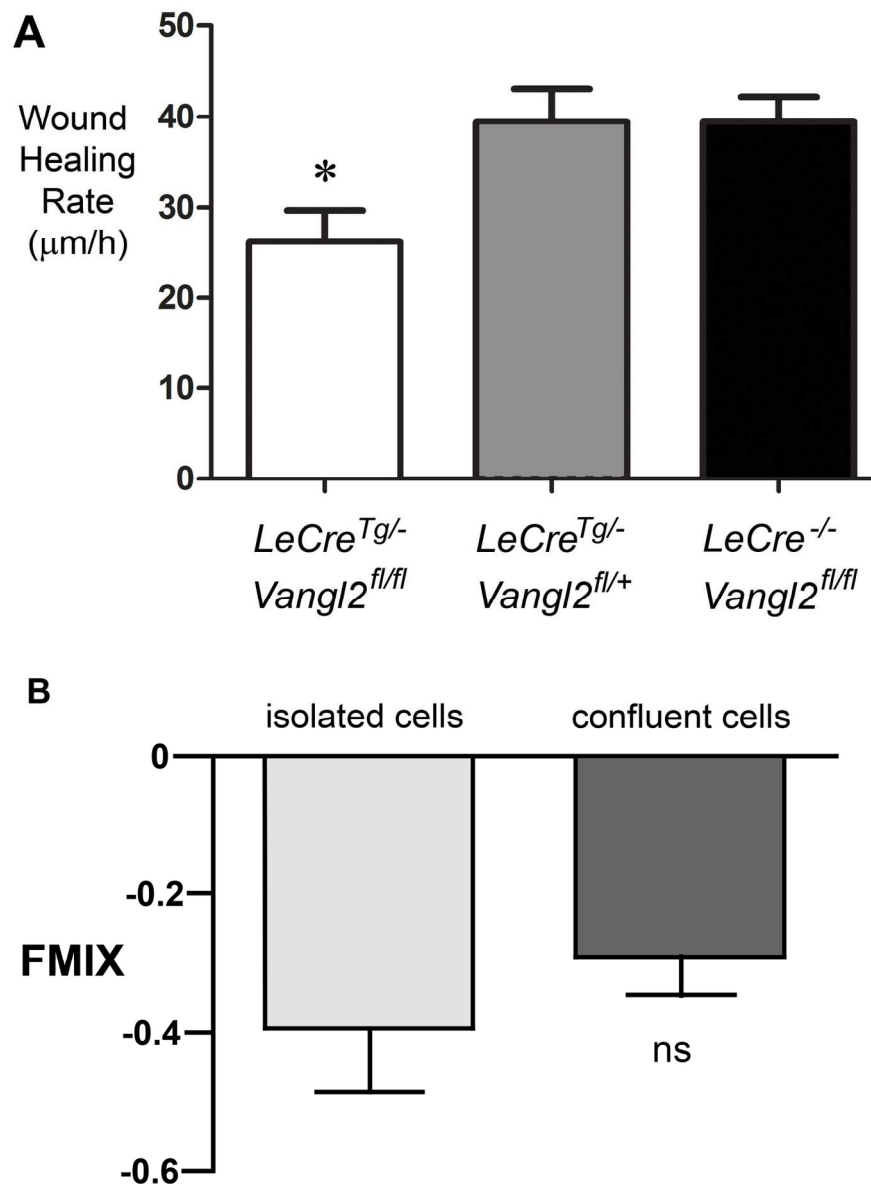
Planar migration defects in Vangl2-deficient corneal epithelial cells. (A) Wound healing rate of in vitro cultured adult mouse corneal epithelial cells. The rate of migration of Le-CreTg/- Vangl2fl/fl cells following scratch-wounding was significantly slower than that of Le-CreTg/- Vangl2fl/+ and Le-Cre-/- Vangl2fl/fl cells. (One-way ANOVA: F = 3.720, P = 0.0309). (B) Cathodal migration (expressed as forward migration index – FMIX – as described in Materials and Methods), for human corneal epithelial cells after VANGL2 knockdown to ~30% of normal protein levels. The response of cell cultured at low density (individual cells) (light grey) was not significantly different from that of confluent cells (dark grey).

134x183mm (300 x 300 DPI)

The core Planar Cell Polarity gene, *Vangl2*, maintains apical-basal organisation of the corneal epithelium.

D. Alessio Panzica*, Amy S. Findlay*, Rianne van Ladesteijn & J. Martin Collinson†
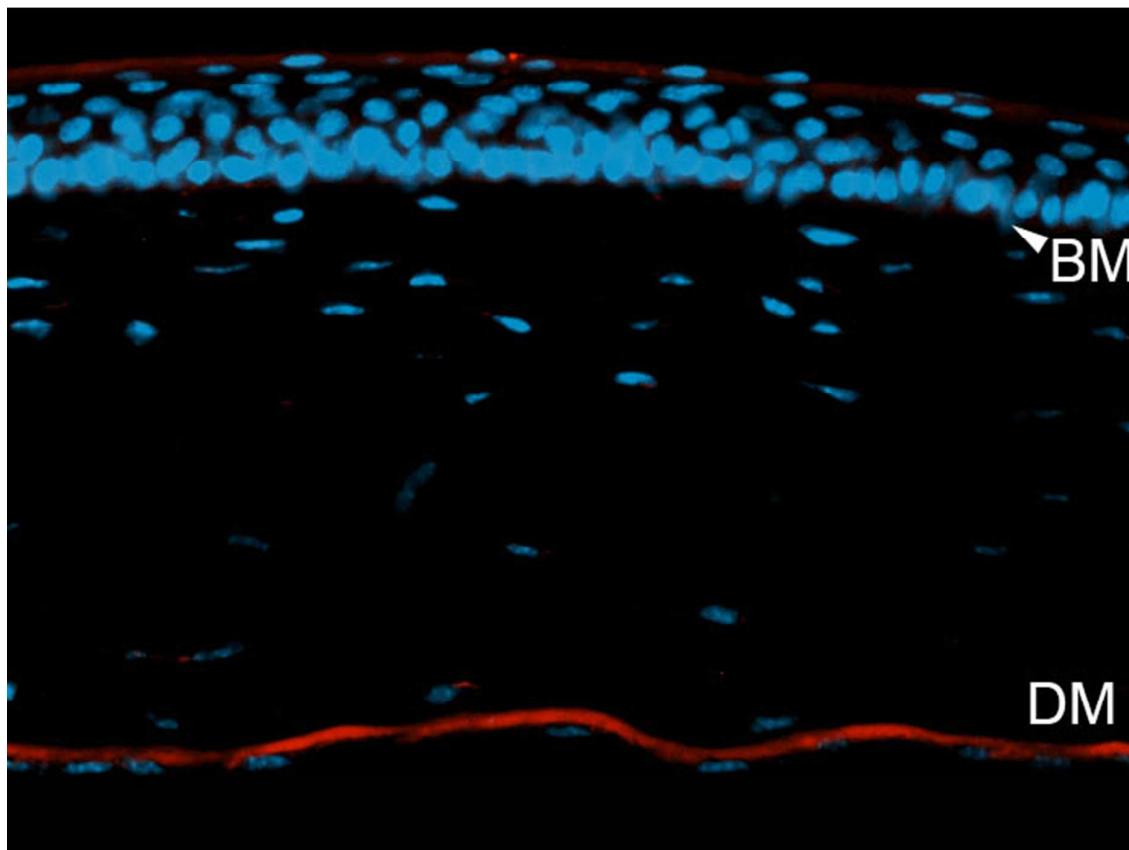
*These authors contributed equally to this work.

† Corresponding author.

J Martin Collinson
School of Medical Sciences,
University of Aberdeen,
Institute of Medical Sciences
Aberdeen AB25 2ZD
UK

Email: m.collinson@abdn.ac.uk

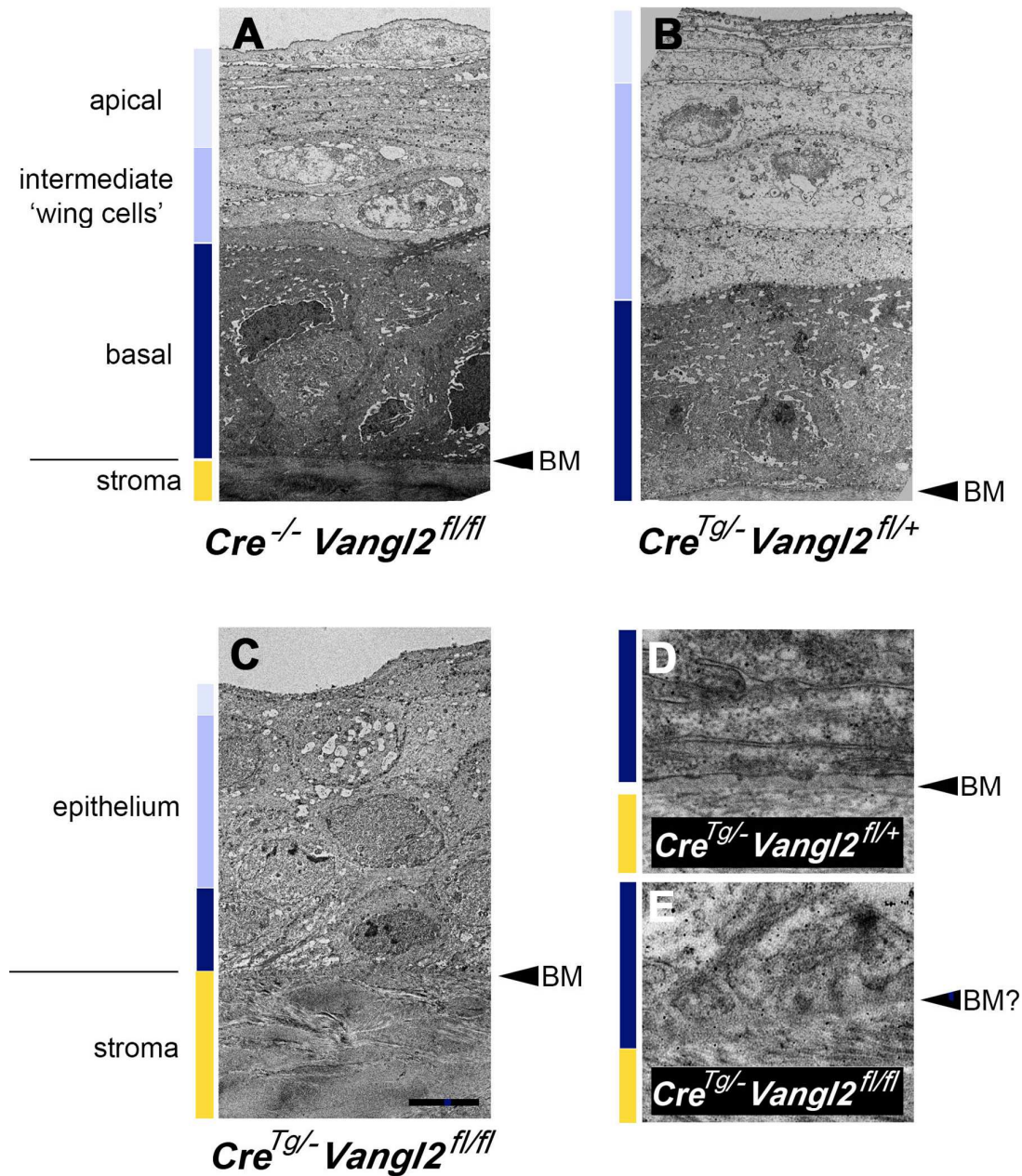Running title: Vangl2 in the cornel epithelium

1

Supplementary Figure 1

Legend: Collagen IV immunostaining of *Le-Cre$^{Tg/-}$ Vangl2$^{fl/fl}$* conditional knockout cornea showing that although ColagenIV was absent from the epithelial basement membrane (BM, arrowhead) it was still detectable in Descemet's membrane (DM)

Supplementary Figure 2

apical

intermediate 'wing cells'

basal

stroma

◄BM

Cre$^{-/-}$ Vangl2$^{fl/fl}$

◄BM

Cre$^{Tg/-}$ Vangl2$^{fl/+}$

epithelium

stroma

◄BM

Cre$^{Tg/-}$ Vangl2$^{fl/fl}$

◄BM

Cre$^{Tg/-}$ Vangl2$^{fl/+}$

◄BM?

Cre$^{Tg/-}$ Vangl2$^{fl/fl}$

Legend: Transmission electron microscopy of control and Vangl2-mutant corneas. A) Transmission electron microscope image of the corneal epithelium of a *Le-Cre*-negative mouse. Corneal stroma, the basal, intermediate and apical epithelial cells are labelled at left. The junction between the basal epithelial cells and the underlying stroma is highlighted with an arrowhead (right). Cytoplasm of the basal layers of cells is electron dense. Suprabasal 'wing' epithelial cells and superficial flattened desquamating cells are visible. **(B)** Comparable image from *Le-Cre$^{Tg/-}$ Vangl2$^{fl/+}$* control mouse showing apical-basal organisation similar to that of *Le-Cre*-negative mice (A). **(C)** Comparable image

from *Le-Cre*$^{Tg/-}$ *Vangl2*$^{fl/fl}$ conditional knockout mouse showing disrupted apical-basal organisation. The epithelium is thin and cells in all layers are of superficially similar shape. The proliferative basal cells are neither electron-dense nor overtly polarised, unlike the controls. **(D)** High magnification image of the basement membrane of a *Le-Cre*$^{Tg/-}$ *Vangl2*$^{fl/+}$ control corneal epithelium showing clear differentiation between the epithelial cells (top) and the underlying stromal collagen fibres (bottom). Basement membrane is denoted by an arrowhead. There is a thin, electron-dense basal lamina directly under the epithelial cells overlying a distinct basement membrane. **(E)** Comparable image to (D) from a *Le-Cre*$^{Tg/-}$ *Vangl2*$^{fl/fl}$ conditional knockout. The boundary between the epithelial cells and stromal collagen (at the level of the arrowhead) is indistinct, with no electron-dense lamina.